Paleomagnetic, structural, and stratigraphic constraints on transverse fault kinematics during basin inversion: The Pamplona Fault (Pyrenees, north Spain)

Juan Cruz Larrasoaña,[1,2,3] Josep María Parés,[4] Héctor Millán,[2] Joaquín del Valle,[5] and Emilio Luis Pueyo[1,2,6]

Received 5 August 2002; revised 6 May 2003; accepted 6 August 2003; published 5 December 2003.

[1] The Pamplona Fault in the Pyrenees is a major transverse structure that has been classically interpreted as a strike-slip fault. However, lack of consensus concerning the sense of movement casts doubt on its actual kinematics and, as a consequence, its role in the Cenozoic evolution of the Pyrenees remains controversial. In order to assess its kinematics, we have conducted a paleomagnetic, structural, and stratigraphic study focused on the Mesozoic and Tertiary sedimentary rocks that outcrop around the southern segment of the fault. Restoration of balanced cross sections allows us to examine the present-day spatial relationship of the sedimentary sequences on both sides of the fault and to reconstruct the geometry of the extensional basins formed during Mesozoic rifting episodes in the Bay of Biscay and Pyrenean domains. Paleomagnetic results indicate that no significant tectonic rotations occurred around the fault during Tertiary inversion of the Pyrenees. The lack of tectonic rotations and revaluation of previous hypotheses argues against a strike-slip movement of the fault. We propose a new model in which the Pamplona Fault is treated as a large-scale ''hanging wall drop'' fault whose kinematics was determined by variations in the geometry and thickness of Mesozoic sequences on both sides of the fault. These variations influenced the geometry of the thrust sheet developed during Tertiary compression. We are unaware of any other transverse fault that has been interpreted in this fashion; thus the Pamplona Fault serves as a case study for the evolution of transverse faults involved in basin inversion processes. *INDEX TERMS:* 1525 Geomagnetism and Paleomagnetism: Paleomagnetism applied to tectonics (regional, global); 8102 Tectonophysics: Continental contractional orogenic belts; 8010 Structural Geology: Fractures and faults; 9604 Information Related to Geologic Time: Cenozoic; 9335 Information Related to Geographic Region: Europe; *KEYWORDS:* transverse fault, basin inversion, paleomagnetism, balanced cross section, Pyrenees. **Citation:** Larrasoaña, J. C., J. M. Parés, H. Millán, J. del Valle, and E. L. Pueyo, Paleomagnetic, structural, and stratigraphic constraints on transverse fault kinematics during basin inversion: The Pamplona Fault (Pyrenees, north Spain), *Tectonics*, *22*(6), 1071, doi:10.1029/2002TC001446, 2003.

1. Introduction

[2] Transverse faults that are oriented parallel or oblique to the tectonic transport direction in mountain belts accommodate variations in the structural style and in along-strike shortening or extension of the belts. While the study of mountain belts has been mostly focused on cross sections perpendicular to their trends [e.g., *Butler*, 1982; *Boyer and Elliot*, 1982; *Wernicke*, 1985; *Lister et al.*, 1986; *McClay*, 1992; *Brun and Beslier*, 1996], the role of transverse faults in mountain belt formation is not yet fully understood. Although 3-D structural, geophysical and analogue modeling data have provided new insights into the role of transverse faults in collisional [e.g., *Laubscher*, 1985; *Mitra*, 1988; *McDougall and Kahn*, 1990; *Thomas*, 1990; *Calassou et al.*, 1993] and extensional settings [e.g., *Harding et al.*, 1985; *Ebinger et al.*, 1987; *McClay and Khalil*, 1998; *Acocella et al.*, 1999], the geometry and deformation mechanisms associated with transverse faults during basin inversion is relatively unknown [see *Cooper and Williams*, 1989; *Buchanan and Buchanan*, 1995].

[3] The Pyrenean mountain belt is a double-verging orogen located at the boundary between the Iberian and the European plates. From Late Cretaceous to Miocene time, the oblique convergence, collision and subduction of Iberia underneath Europe [*Srivastava et al.*, 1990; *Muñoz*, 1992; *Pulgar et al.*, 1996] caused the end of sea-floor spreading in the Bay of Biscay and the initiation of compression along the northern Iberian margin, leading to inversion of Mesozoic extensional basins and ultimately to uplift of the Pyrenees [e.g., *Muñoz*, 1992; *Choukroune*, 1992]. In the central eastern part of the belt, the core of the orogen is formed by Paleozoic rocks of the Axial Zone,

[1]Paleomagnetic Laboratory, Institute of Earth Sciences ''Jaume Almera'', Consejo Superior de Investigaciones Científicas, Barcelona, Spain.
[2]Department of Earth Sciences, University of Zaragoza, Zaragoza, Spain.
[3]Now at the Southampton Oceanography Centre, Southampton, UK.
[4]Department of Geological Sciences, University of Michigan, Ann Arbor, Michigan, USA.
[5]Santo Domingo 3, Lekeitio, Spain.
[6]Now at Laboratoire de Méchanismes de Transfert en Géologie, Université Paul Sabatier, Toulouse, France.

0278-7407/03/2002TC001446

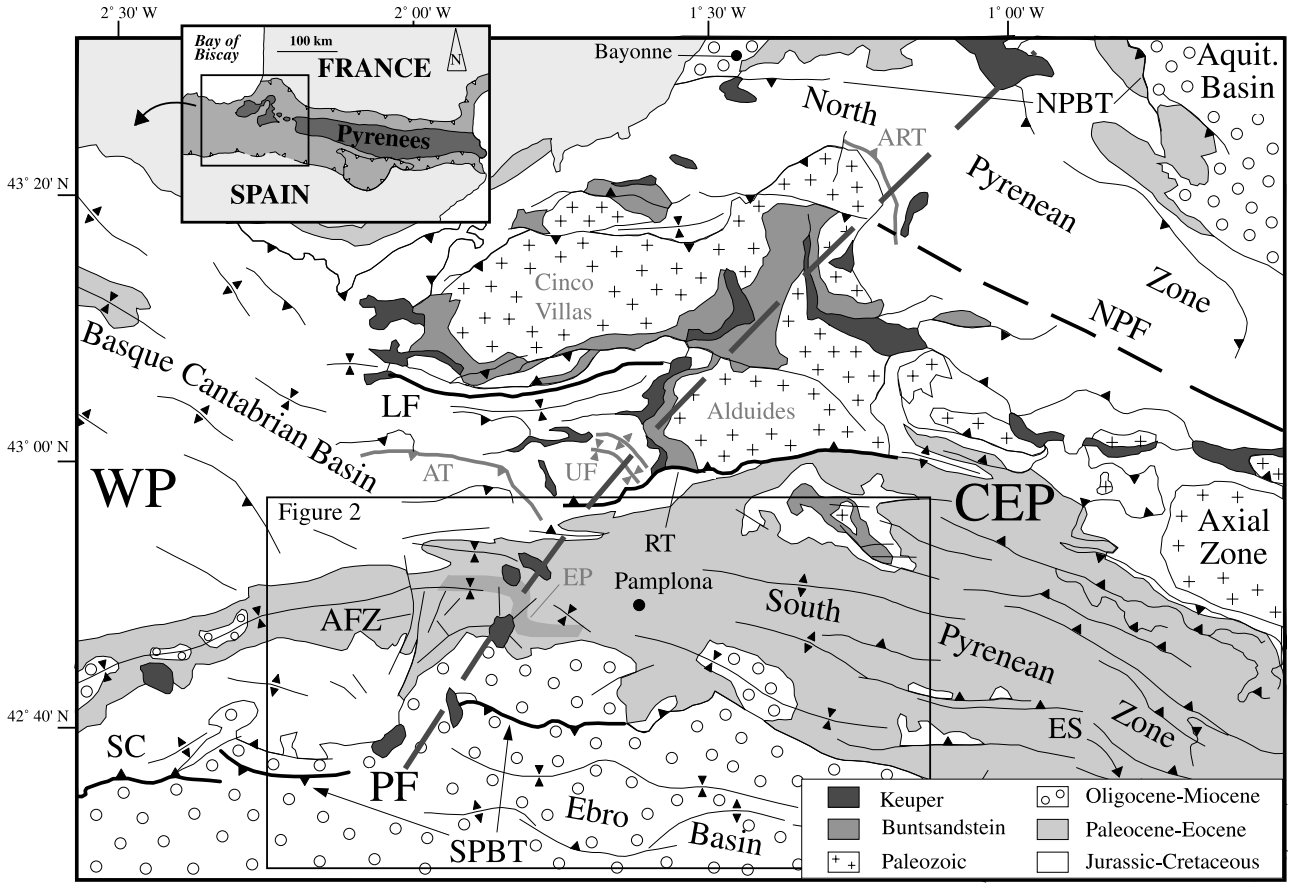

Figure 1. Geological sketch map of the transition between the central eastern Pyrenees (CEP) and western Pyrenees (WP), with the location of the studied area. The main features used to infer the sinistral displacement along the Pamplona Fault are shown in black, whereas those claiming a dextral displacement are shaded. PF, Pamplona Fault; NPF: North Pyrenean Fault; LF, Leiza Fault; SPBT: south Pyrenean basal thrust; NPBT, north Pyrenean basal thrust; AFZ, Andia Fault Zone; RT, Roncesvalles thrust; ART: Arberoue thrust; UF, Ulzama folds; AT, Aralar thrust; EP, Eocene platforms; SC, Sierra de Cantabria; ES, external Sierras.

which are bounded to the north by the deep-seated North Pyrenean Fault (NPF) [e.g., *Debroas*, 1990; *Choukroune*, 1992]. The North Pyrenean Zone, which is mainly constituted by Mesozoic rocks, overrides the Aquitaine foreland basin to the north. South of the Paleozoic Axial Zone, the South Pyrenean Zone constitutes the external part of the belt that overrides the foreland basin located to the south (Ebro basin). South vergent thrusts and folds appear both in the Axial and in the South Pyrenean Zones, whereas north vergent structures characterize the North Pyrenean Zone. The western Pyrenees constitute the Basque-Cantabrian basin. Although south vergent structures are also found in this area, mostly along the southern margin overriding the Ebro basin, north vergent folds and thrusts are the main structural features in the central and northern areas of the Basque-Cantabrian mountains. North vergent structures are also predominant offshore in the Bay of Biscay [e.g., *Soler et al.*, 1981; *Alvarez-Marrón et al.*, 1997]. The earliest compressional structures formed in the core of the central eastern domain in the uppermost Cretaceous [*Puigdefàbregas et al.*, 1992; *Muñoz*, 1992]. As deformation proceeded, thrust systems propagated toward the foreland and former foreland basins became progressively involved in the deformation front as piggyback basins [*Puigdefàbregas et al.*, 1992; *Muñoz*, 1992]. The external zones of the Pyrenean orogen developed in a ''thin-skinned'' fashion, where the upper Triassic plastic levels (Keuper facies) acted as a main detachment horizon in the North and South Pyrenean Zones and also in the Basque-Cantabrian mountains [e.g., *Muñoz*, 1992].

[4] The Pamplona Fault (PF) is a major NNE-SSW trending transverse structure that delineates the boundary between the central eastern and the western Pyrenees [*Muñoz et al.*, 1983] (Figure 1). The PF has undergone a complex tectonic evolution since the Late Paleozoic [*Rat*, 1988; *Martínez-Torres*, 1989; *Turner*, 1996; *Faci et al.*, 1997]. The PF is a Late-Variscan structure that behaved as an extensional transfer fault during the Mesozoic and was subsequently involved in the Tertiary compression responsible for the uplift of the Pyrenean belt. The kinematics of the PF during Tertiary compression is not well understood.

Some interpretations suggest a sinistral displacement [*Engeser and Schwentke*, 1986; *Rat*, 1988; *Frouté*, 1988; *Faci et al.*, 1997], although there are also interpretations supporting dextral [*Müller and Roger*, 1977; *Turner*, 1996; *Payros*, 1997] and even combined [*Martínez-Torres*, 1989] movements. The tectonic complexity of the area and the scarcity of detailed structural and geophysical data have prevented the understanding of the relationship and kinematics of the PF and associated structures, leading to contradictory interpretations about its role in what is a key location for understanding the Pyrenean orogen.

[5] In this paper, we present a combined paleomagnetic, structural and stratigraphic study of the external units of the Pyrenees in the transition between its central eastern and western domains, where the PF is located. Paleomagnetic data provide a test for the different hypotheses concerning the kinematics of the PF during the Tertiary. Structural and stratigraphic data have been used to examine the present-day spatial relationship of the sedimentary sequences on both sides of the fault and to reconstruct the original geometry of the Mesozoic extensional basins. We propose a new model for the PF that explains the overall data in terms of a basin inversion mechanism.

2. Pamplona Fault

[6] The PF (also named the Estella-Dax or Estella fault) can be traced for more than 120 km by a NNE-SSW alignment of Triassic salt diapirs [*Brinkmann and Logters*, 1967] (Figure 1). Along its northern segment, the PF runs through the Paleozoic Basque massifs of Alduides and Cinco Villas, which are Paleozoic basement units equivalent to those in the Axial Zone [*Rat*, 1988; *Turner*, 1996; *Souriau and Pauchet*, 1998]. At its southern termination, the PF cuts along the Mesozoic and Tertiary cover units. Although the fault is not clearly visible at the surface because the cover is detached at the upper Triassic plastic levels, it can be traced by a diffuse alignment of shallow (5–10 km) earthquakes [*Souriau and Pauchet*, 1998] and by the presence of upper Triassic salt diapirs and the so-called Andia Fault Zone (AFZ) [*Faci et al.*, 1997]. The origin of the PF is related to the fracture network developed within the European basement during the latest stages of the Variscan (Late Carboniferous) orogeny [*Mattauer*, 1968; *García-Mondéjar*, 1996]. During the Mesozoic, mainly in the lower Cretaceous, a sequence exceeding 10 km in thickness was deposited in the western Pyrenees in connection with the opening of the Bay of Biscay as a subsidiary branch of the North Atlantic rift [*García-Mondéjar*, 1996]. In contrast, a sequence of less than 4000 m of Mesozoic sediments was deposited around most of the central eastern Pyrenees [*Vergès and García-Senz*, 2001]. The PF can therefore be interpreted as a transfer fault that separated two segments of the Pyrenean rift, the Pyrenean mountains and the Bay of Biscay domain, where differences in the amount and style of extension probably occurred. This transfer fault might have represented the continuation in the continental crust of a transform fracture of the Pyrenean rift [see *Engeser and Schwentke*, 1986; *Boillot and Malod*, 1988]. Although the PF may have undergone strike-slip movement during the Mesozoic, no clear evidence supporting this possibility has been found to date [*García-Mondéjar*, 1996].

[7] Several interpretations have been proposed for the role of the PF during the Pyrenean orogeny. The PF is considered to cause the ~30 km of sinistral offset observed between the NPF in the central eastern Pyrenees and its prolongation into the western Pyrenees, the Leiza Fault (LF) [e.g., *Engeser and Schwentke*, 1986; *Rat*, 1988; *Faci et al.*, 1997] (Figure 1). A sinistral offset has been also suggested to explain the presence, in the southern part of the western Pyrenees, of north vergent structures and thick lower Cretaceous sequences typical from the North Pyrenean Zone [*Martínez-Torres*, 1989]. Further evidence supporting a sinistral displacement is the offset of the south Pyrenean basal thrust observed at the southern tip of the PF [*Froutè*, 1988]. In contrast, some authors have proposed that the PF behaved as a dextral strike-slip fault to explain the curvature of some structures located above the trace of the PF, e.g., the Ulzama, Aralar and Arberoue structures [*Müller and Roger*, 1977; *Schoeffler*, 1982; *Martínez-Torres*, 1989] (Figure 1). The "Z-type" bending of Eocene facies across the southern part of the PF has been interpreted by *Payros* [1997] as additional evidence for dextral displacement. Moreover, the relative position of the Cinco Villas and Alduides basement units across the PF has been also considered to favor a dextral movement across the fault [*Turner*, 1996]. *Martínez-Torres* [1989] integrated available kinematic data and proposed that the PF accommodated different senses of displacement at different times. Sinistral displacement would have occurred during the Eocene in relation to formation of north vergent structures west of the PF [*Martínez-Torres*, 1989]. The PF would have later undergone dextral movement associated with the main Pyrenean deformation event occurred in the area during Oligocene-Miocene times [*Muñoz-Jiménez and Casas-Sainz*, 1997]. This model has the appeal of linking directional movements with different episodes of deformation. However, the variety of arguments used to establish the kinematics of the PF at different stages during Tertiary compression and the chronological inconsistencies between the different models raise doubts about the overall set of kinematic interpretations. For example, the sinistral movement invoked by *Martínez-Torres* [1989] in connection with the formation of Eocene north vergent structures is incompatible with the dextral displacement proposed by *Payros* [1997] at the same time. Similarly, both *Faci et al.* [1997] and *Turner* [1996] link the sinistral and dextral movements with the main Oligocene-Miocene compression, respectively.

[8] The PF has been classically considered as a first-order structural feature of the Pyrenean orogen, and has been claimed to represent a classic example of a transverse structure at the lateral termination of a mountain belt where switches in subduction polarity (e.g., Iberia underneath Europe in the central eastern Pyreness versus oceanic crust of the Bay of Biscay underneath Iberia in the western Pyrenees) have occurred [*Turner*, 1996]. It appears, however, that the kinematics of the PF need to be clarified

before its role in the evolution of the Pyrenean orogen can be properly assessed.

3. Structural Data

[9] In the studied area, the Jaca-Pamplona basin and the Miranda-Urbasa syncline represent the central eastern and western Pyrenees, respectively (Figure 2). The geometry of these units is depicted in Figure 3 along two balanced cross sections broadly perpendicular to the main structural trends (see Figure 2 for location). The sections have been extended farther south into the Ebro foreland basin to provide a complete view of the deformation front. To construct the sections, we used surface geological data available from maps published by the Spanish Geological Survey [*Instituto Geológico y Minero de España* (*IGME*), 1977a, 1977b, 1978a, 1978b, 1978c, 1987a, 1987b, 1987c, 1987d, 1987e, 1987f, 1987g], the synthesis of the geology of Navarra [*Faci et al.*, 1997], previous stratigraphic and structural studies [*Riba et al.*, 1983; *Froutè*, 1988; *Serrano and Martínez del Olmo*, 1989; *Riba and Jurado*, 1992; *Casas-Sainz et al.*, 1994; *Payros*, 1997; *Cortés-Gracia and Casas-Sainz*, 1997; *Muñoz-Jiménez and Casas-Sainz*, 1997], and our own structural observations. Borehole data published by *IGME* [1990] and seismic lines compiled by *Serrano and Martínez del Olmo* [1989] and *Muñoz-Jiménez and Casas-Sainz* [1997] have been used to constrain the structure at depth. The Mesozoic and Tertiary marine formations have variable thickness, although their distribution and lateral variations are well constrained due to the presence of several boreholes. Continental Tertiary deposits also have lateral variations in facies and thickness.

[10] The south Pyrenean basal thrust (SPBT) does not emerge to the surface and thus its geometry cannot be unambiguously established. However, the proposed cross sections satisfy the available surface and subsurface data and are consistent in terms of conservation of areas and bed length. In the studied area, the Jaca-Pamplona basin and the Miranda-Urbasa syncline constitute south vergent synclinoria that are detached at upper Triassic levels. These synclinoria have small, steep northern limbs and longer, either subhorizontal (Figure 3a) or gently dipping southern flanks (Figure 3b) that represent monoclinal flexures of the culmination limbs associated with the frontal thrust system. A total shortening of ~15.6 km can be estimated for the Pamplona transect after restoration of the cross section back to its condition prior to Tertiary compression (Figure 4). Along the Pamplona transect, the Tafalla thrust and the folds located in the central sector of the Ebro basin (Arguedas and Falces anticlines) are detached in the middle Oligocene Falces Gypsum Formation [*Casas-Sainz et al.*, 1994] and accommodate a total shortening of about 8–9 km. Development of such folds in the foreland requires that the evaporites increase their thickness toward the center of the Ebro basin, which is consistent with paleogeographical data [*Riba and Jurado*, 1992]. Most of the tectonic displacement along the SPBT appears to have been transferred to the footwall at the level of the Falces Formation, with subsidiary shortening being accommodated at the Puente la Reina back thrust, which is rooted in the lowermost Oligocene Puente la Reina Gypsum Formation [*Faci et al.*, 1997]. The geometry of the SPBT is controlled by the presence of different detachment levels. After a hanging wall flat in upper Triassic units and a hanging wall ramp in Mesozoic and Tertiary marine sequences, it is detached in the Puente la Reina Gypsum Formation. This formation consists of marls and evaporites that give way to sandstones and marls toward the south [*Riba and Jurado*, 1992]. This stratigraphic variation probably caused a mechanical impediment for the SPBT to proceed, which was then forced to ramp up through the Tertiary stratigraphic section until it reached the Falces Formation, where a third detachment formed.

[11] Surface data suggest that similar structures could also be present in the Urbasa transect (Figure 3b). We interpret that the geometry of the SPBT is controlled by a previous Mesozoic normal fault and by the arrangement of the evaporitic units (e.g., upper Triassic, Puente la Reina and Falces formations). As it is the case in the Pamplona transect, the basal thrust climbs up through the Mesozoic-upper Eocene deposits. The detachment continues over a flat located in the Oligocene Puente la Reina Formation and finally ramps through the continental deposits to reach the Falces Formation, forming the upper flat. In the upper ramp, the thrust places a hanging wall ramp in upper Triassic strata over a footwall ramp in the Oligocene deposits of the Puente la Reina Formation. This displacement is transferred to the upper flat where it is taken up by contractional structures detached over the evaporites of the Falces Formation. Part of the shortening along the Urbasa section is accommodated by the Barbarín thrust (~3 km of horizontal shortening), which places a hanging wall ramp in Cretaceous rocks over a footwall ramp in Tertiary continental deposits. This thrust may be considered as a hanging wall shortcut whose location and attitude was controlled by a previous Mesozoic extensional fault. To the north of the Barbarín thrust, the structure is defined by two south verging folds: the Gastiain anticline and the Miranda-Urbasa syncline. The former has been interpreted as the result of buttressing of an extensional structure that has not

Figure 2. (opposite) Geological map of the studied area with the location of paleomagnetic sampling sites. Numbered solid (open) circles indicate the positions of sites where reliable paleomagnetic data (no data) were obtained. Bold numbers indicate the structural units into which the studied area has been divided: 1, Liédena anticline; 2, Lumbier (eastern Izaga) syncline; 3, Izaga syncline; 4, Alaiz; 5, Pamplona synclinorium; 6, Añezkar syncline; 7, Ibero syncline; 8, San Donato syncline; 9, Goñi syncline; 10, Abárzuza block; 11, Urbasa syncline. AFZ, Andia Fault Zone; ED, Estella diapir; AD, Alloz diapir; SD, Salinas de Oro diapir; TD, Arteta diapir; ND, Anoz diapir; ID, Iza diapir. The locations of the cross sections in Figures 3 and 5 are also shown.

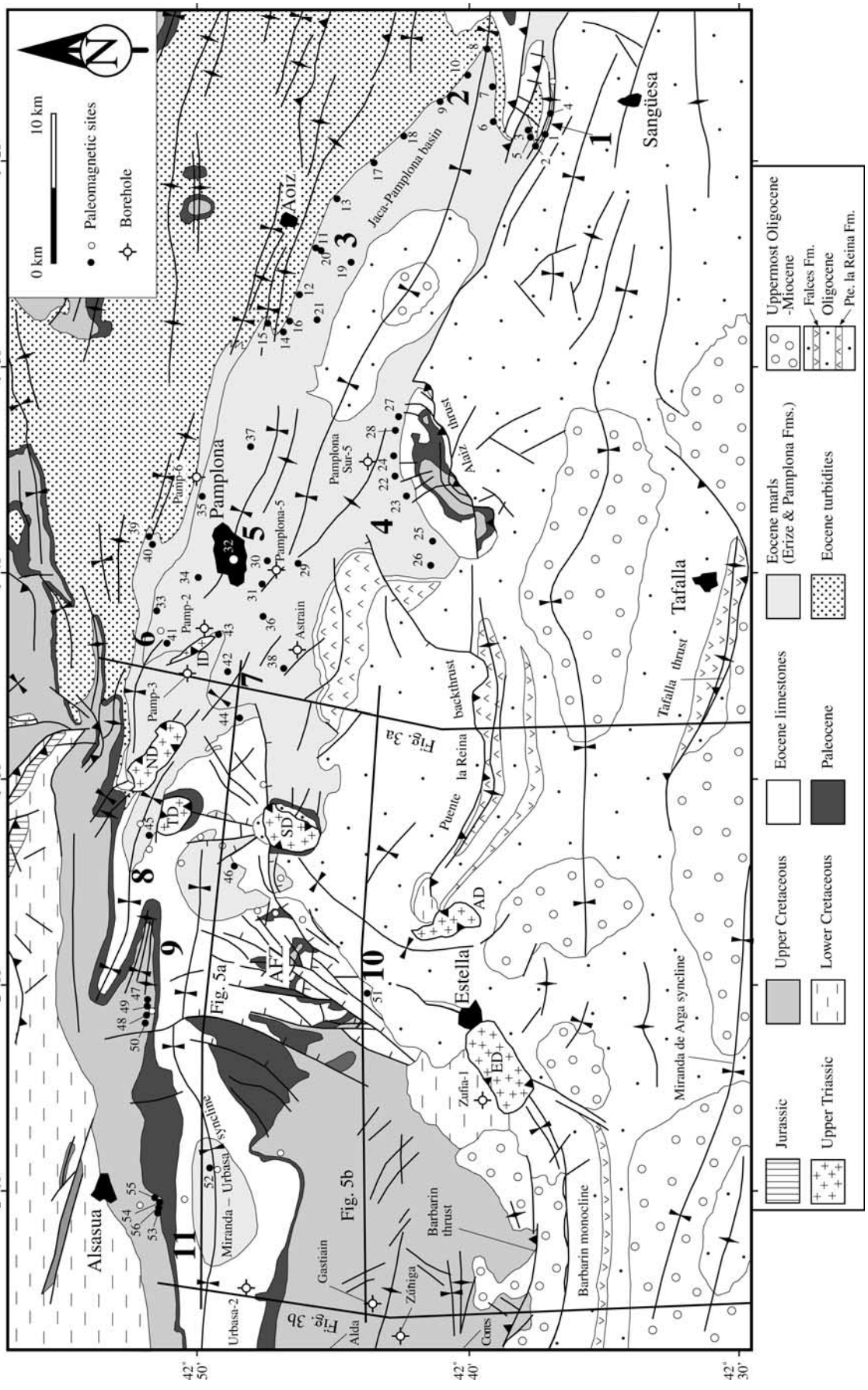
N
0 km
10 km
Paleomagnetic sites
Borehole
Alsasua
Miranda – Urbasa syncline
Urbasa-2
Gastiain
Zúñiga
Alda
Barbarin thrust
Barbarin monocline
Fig. 3b
Fig. 5b
Fig. 5a
AFZ
Pamplona
Pamp-6
Pamp-2
Pamp-3
Pamplona-5
Pamplona Sur-5
Astrain
ID
ND
TD
SD
AD
ED
Zufia-1
Estella
Puente la Reina
backthrust
Fig. 3a
Aoiz
Jaca-Pamplona basin
Alaiz thrust
Tafalla
Tafalla thrust
Miranda de Arga syncline
Sangüesa
Cores
Jurassic
Upper Triassic
Upper Cretaceous
Lower Cretaceous
Eocene limestones
Paleocene
Eocene marls (Erize & Pamplona Fms.)
Eocene turbidites
Uppermost Oligocene -Miocene
Falces Fm.
Oligocene
Pte. la Reina Fm.
2° 10'
2° 00'
1° 50'
1° 40'
1° 30'
1° 20'
42° 50'
42° 40'
42° 30'

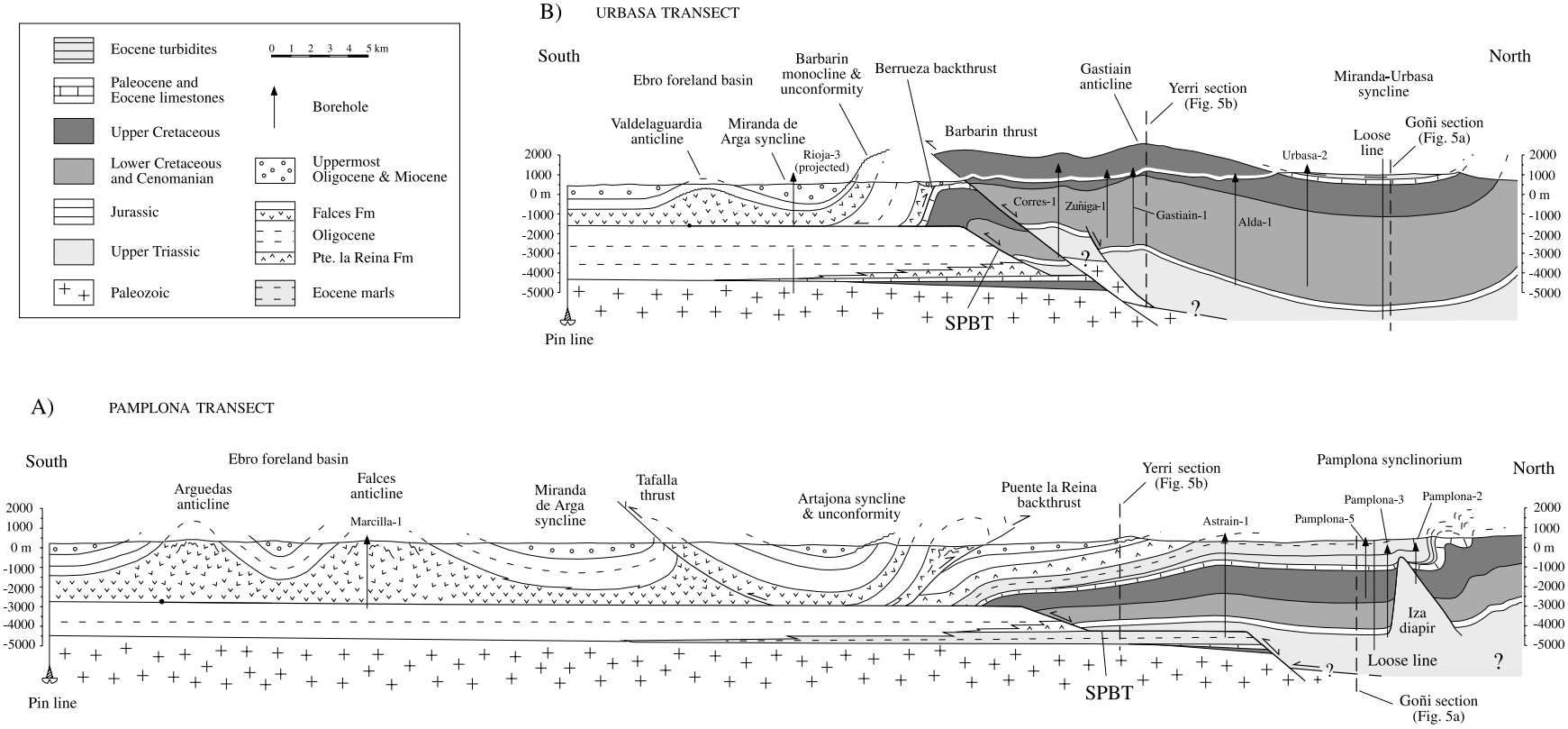

Figure 3. Balanced cross sections of the Jaca-Pamplona basin and the Miranda-Urbasa syncline (see location in Figure 2).

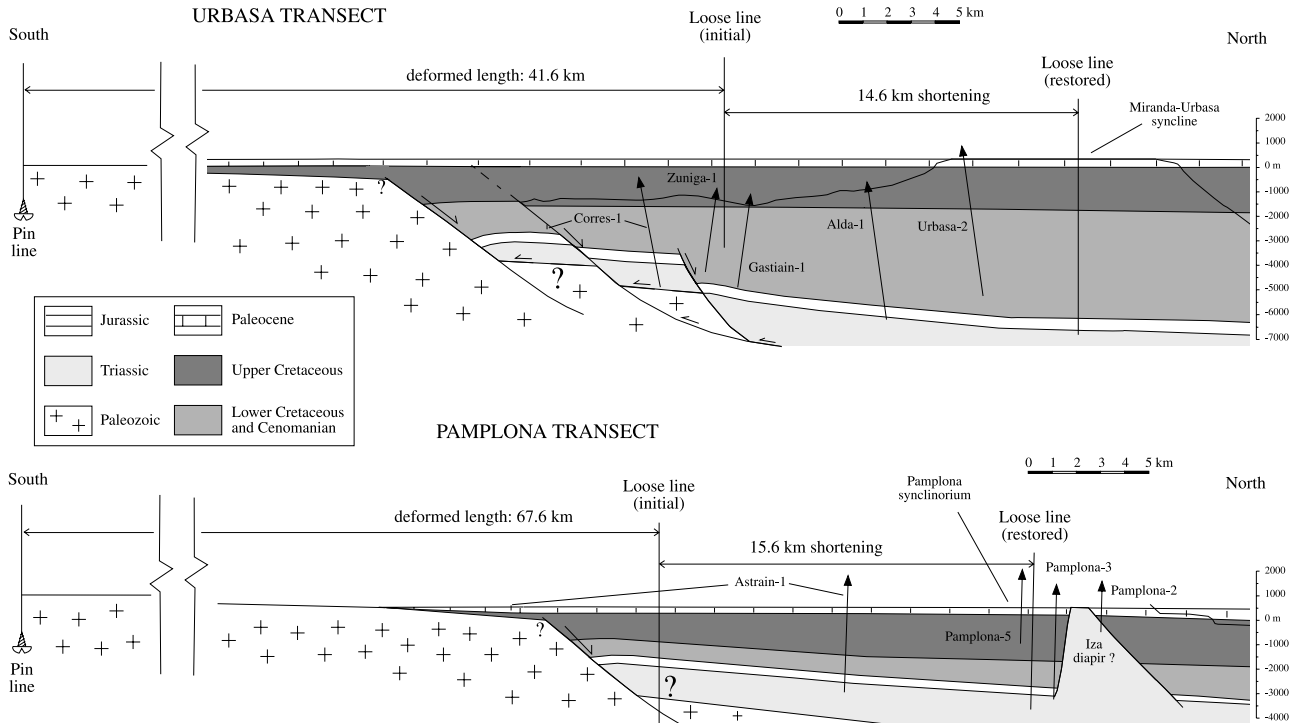

Figure 4. Reconstruction of the Cretaceous extensional basins at the beginning of the Paleocene (prior to development of Tertiary thrusting), based on restoration of the cross sections depicted in Figure 3.

experienced a significant amount of inversion during Tertiary compression.

[12] On the basis of the above, we interpret that part of the shortening measured in the Mesozoic and marine Tertiary allochthonous cover rocks has been accommodated in Oligocene-Miocene rocks by the Berrueza back thrust (covered by Pliocene deposits) and by folding toward the south. Most of the folding is represented by the western prolongation of detachment folding depicted at the southern tip of the Pamplona section. On the other hand, small detachments within the Oligocene sequence might have accommodated a small part of the displacement under the Miranda de Arga syncline [*Muñoz-Jiménez and Casas-Sainz*, 1997]. Total shortening of ~14.6 km can be estimated for the SPBT along the Urbasa transect (Figure 4). This value is similar to the estimated ~15.6 km of shortening for the Pamplona transect and to the ~14 and ~15 km of shortening reported in adjacent areas of the external Sierras [see *Millán et al.*, 2000] and Sierra de Cantabria [*Martínez-Torres*, 1993] (see Figure 1 for location), respectively. According to the cross sections showed in Figure 3 and the syntectonic origin of the Tertiary continental sequences [*Muñoz-Jiménez and Casas-Sainz*, 1997], the main thrusting episode along the Pamplona and Urbasa transects can be dated between upper Oligocene and middle Miocene.

[13] From the reconstruction of the extensional basins at the end of the Mesozoic (Figure 4) it is clear that the main differences observed between the Urbasa and Pamplona transects are related to the thickness of the Cretaceous sediments. Jurassic rocks in both sections have a comparable thickness of less than 500 m. Upper Triassic marls and evaporites constitute the regional detachment level, and therefore it is difficult to assess their original thickness. The thickness of the Cretaceous sediments in the Urbasa transect is more than twice that in the Pamplona cross section. Lower Cretaceous and Cenomanian sediments are less than 1300 m thick to the east of the PF, whereas they reach more than 3500 m in thickness throughout most of the Urbasa section. Upper Cretaceous sequences are also thicker along the Urbasa section, although the difference is not as dramatic as for the lower Cretaceous and Cenomanian. Moreover, the overall thickness of the Cretaceous sediments diminishes progressively in both sections toward the south. In the Sierra de Cantabria, about 30 km west of the studied area, the Rioja-3 borehole was drilled in the foreland just 2 km to the south of the SPBT [*IGME*, 1990]. This hole did not cut Mesozoic sediments between the continental Tertiary deposits and the Paleozoic basement, which was reached at about 4600 m below sea level (mbsl). The Astrain-1 borehole drilled in the Pamplona basin stopped at 4400 mbsl in the marine Tertiary units of the footwall of the SPBT. The fact that the maximum depth of the Paleozoic basement in the area is estimated at somehow less than 5000 mbsl [see *Riba et al.*, 1983] indicates that the Mesozoic sequences must be extremely thin, if present, even close to the SPBT (see Figure 3). In order to explain the contrast between kilometer-scale thicknesses of Cretaceous sediments in the hanging wall of the SPBT and their

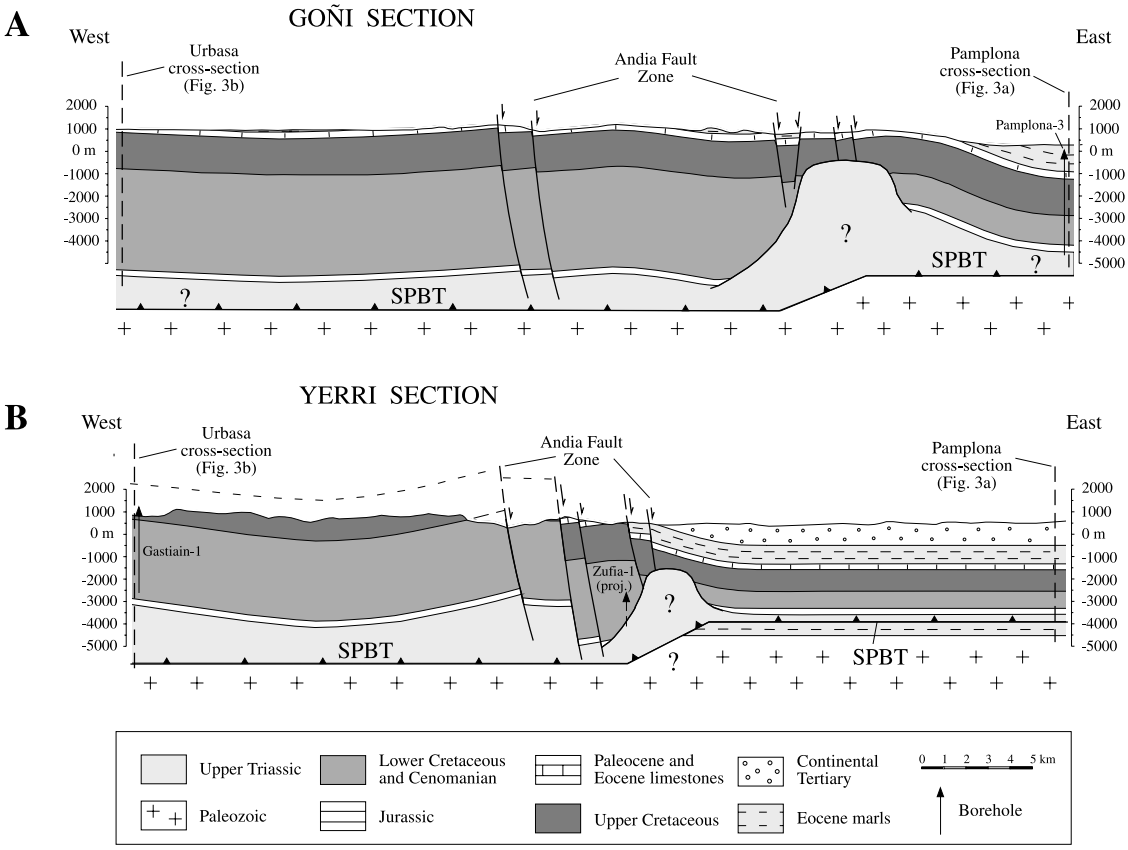

Figure 5. E-W cross sections across the Andia Fault Zone (see location in Figure 2).

disappearance just few km southward, in the footwall, we conclude that the Cretaceous basins were limited by extensional faults and that these extensional faults were reactivated as thrusts planes during Tertiary compression. This agrees with interpretations proposed for other segments of the SPBT along the Basque-Cantabrian basin [*Martínez-Torres*, 1993]. Some of these extensional faults, such as the one interpreted south of the Gastiain anticline in the Urbasa section to explain the striking variations observed in the thickness of the lower Cretaceous and Cenomanian, remained inactive during the Tertiary.

[14] The Andia Fault Zone (AFZ) is located between the Pamplona and Urbasa transects and constitutes an area of extraordinary fault density that has been considered as the surface expression of the PF [*Faci et al.*, 1997; *Liesa*, 2000]. The AFZ has an open-to-the-north fan geometry. The main faults of the system have N to NE orientations and steeply dip to the east. They acted as normal faults that caused the sink of the Mesozoic and Tertiary rocks located at the eastern side of the PF. The maximum vertical displacement associated with individual faults within the AFZ (~2000 m) is found at the southern part of the fault system, where Eocene sediments are in contact with lower Cretaceous rocks. The total vertical displacement diminishes progressively to the north until the faults eventually disappear within a distance of about 20 km. A set of smaller E-W fractures, with normal displacements, interconnects the main faults of the system. Microstructural data indicate that the same orientation and kinematic pattern is found at the outcrop scale [*Liesa*, 2000]. The two E-W cross sections showed in Figure 5 illustrate the geometry and the total vertical displacement accommodated by the AFZ at two positions along transport direction of the SPBT. The upper Triassic salt diapirs located around the AFZ have been active since the Mesozoic, especially during lower Cretaceous, Paleocene and Eocene times [e.g., *Brinkmann and Logters*, 1967; *Wiedmann*, 1979; *Faci et al.*, 1997]. Some of the diapirs (Estella, Alloz, Anoz) have elongated shapes parallel to the main adjacent compressive structures, while others (Arteta, Salinas de Oro) have circular sections with radial fractures. Some of these fractures are physically connected to the main faults of the AFZ and affect Oligocene and Miocene continental sequences, which indicates that both the AFZ and the diapirs were active during the main Oligocene-Miocene thrusting.

4. Paleomagnetism

[15] Paleomagnetic sites have been grouped in 11 structural units, which are located on both sides of the southern segment of the PF and also around the trace of the fault (e.g., within the AFZ). Micropaleontological data have provided an age constraint for the Cretaceous sediments [*Faci et al.*, 1997] and the Eocene limestones [*Payros*, 1997; *Faci et al.*, 1997] from which reliable paleomagnetic results have been obtained. A Bartonian-Priabonian age has

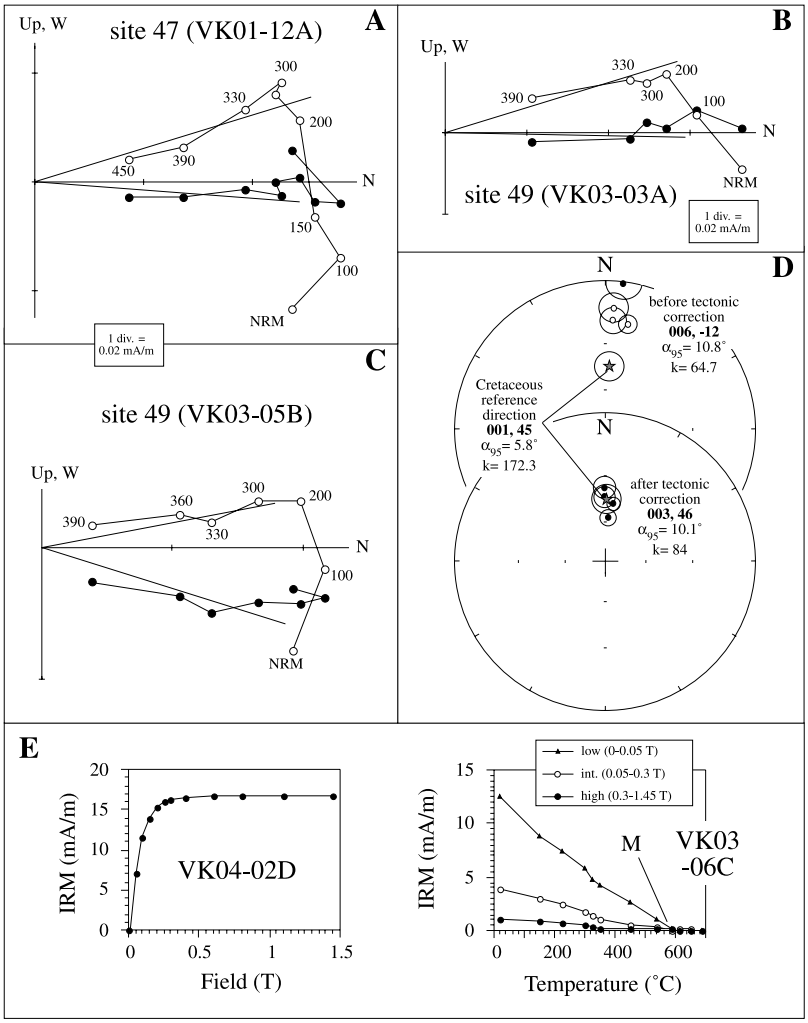

Figure 6. Paleomagnetic results from Santonian marls. (a, b, and c) Representative NRM demagnetization diagrams from the Goñi syncline (all plots are for in situ coordinates). Solid (open) symbols indicate projections onto the horizontal (vertical) plane. The lines represent linear fits to the ChRMs. (d) Equal area projection of site mean directions from the Goñi syncline, with associated α_{95} and k, before and after tectonic correction. The mean value of the four sites is shown for comparison with the upper Cretaceous reference direction. Solid (open) symbols represent lower (upper) hemisphere projections. (e) IRM acquisition and thermal demagnetization results of a three-component IRM of representative Santonian marl samples. M indicates the decay of remanence associated with magnetite.

been established for the Eocene marls according to micropaleontologic and magnetostratigraphic studies [*Canudo et al.*, 1988; *Hogan and Burbank*, 1996; *Payros*, 1997]. All sampled lithologies post-date the Cretaceous rotation of Iberia [see *Van der Voo*, 1993] and predate the main Oligocene-Miocene Pyrenean compression. They can thus be used to unravel the kinematic evolution of the different structural units around the PF during the Pyrenean orogeny. Older lithologies that crop out around the northern segment of the PF were not considered to avoid overprints with rotations that might have occurred during Cretaceous and/or late Variscan times. We sampled 74 sites in several marine formations ranging from upper Cretaceous to Eocene in age (Figure 2). At every site, 8 to 15 standard oriented cores (25.4 mm in diameter) were collected with a portable gas-powered drill, spanning a stratigraphic section of up to 15 m. Magnetic remanence measurements were made using a GM400 three-axis cryogenic magnetometer at the IES Jaume Almera (CSIC, Barcelona) and using 2G cryogenic magnetometers at the Ludwig Maximilians University (Munich, Germany) and at the University of Michigan (Ann Arbor, USA). The noise level of these magnetometers is less than 7×10^{-6} A/m, which is much lower than the magnetization of the measured samples. Between 9 and 15 samples per site were subjected to stepwise thermal demagnetization of the natural remanent magnetization (NRM) using Schonsted and ASC furnaces. This process involved between 8 and 14 steps at intervals of 50°, 30°, and 20°C to

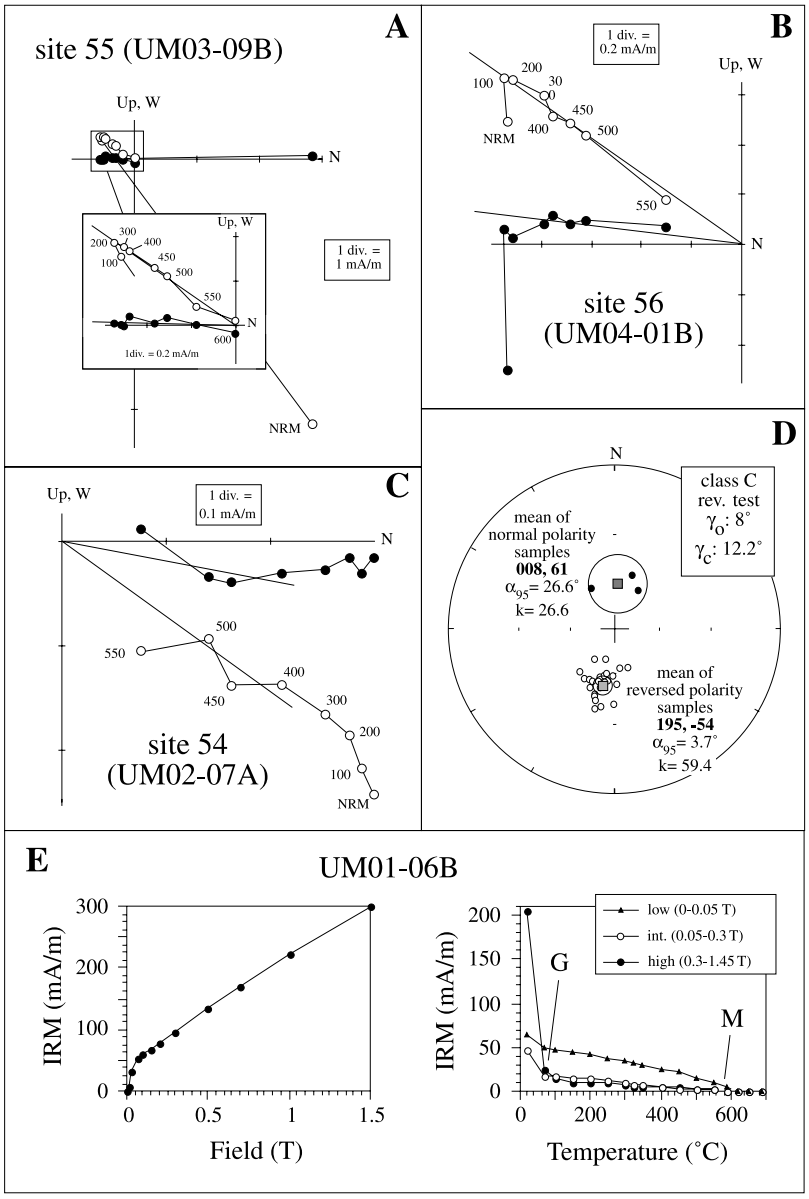

Figure 7. Paleomagnetic results for Maastrichtian limestones. (a, b, and c) Representative NRM demagnetization diagrams from the Urbasa syncline (all plots for in situ coordinates). (d) Positive reversal test performed with the ChRMs from the Urbasa syncline. Here γ_0 is the angular difference between normal and reversed mean directions, whereas γ_c represents the critical value of the angle at which the test is considered negative. All symbols are as in Figure 4. (e) IRM acquisition and thermal demagnetization results of a three-component IRM of representative Maastrichtian limestone samples. G and M indicate the decay of remanence associated with goethite and magnetite, respectively.

a maximum temperature of up to 600°C. Formation of new magnetic phases at high temperatures often prevented the complete demagnetization of the samples. However, characteristic remanent magnetization (ChRM) directions with linear paths directed toward the origin of the orthogonal plots could be identified in most (~75%) of the samples (see Figures 6–9). We used principal component analysis [*Kirschvink*, 1980] and Fisher statistics [*Fisher*, 1953] to calculate ChRM directions and site mean paleomagnetic vectors, respectively. The combination of individual ChRM directions with demagnetization circles [*Bailey and Halls*, 1984] was also used, as described by *McFadden and McElhinny* [1988], to compute mean directions for a few sites from Eocene marls where the limited number of linear vectors hampered the calculation of reliable site mean directions (see Table 1). The plunge of folds (<13° except in one case) was restored to the horizontal before applying tilt correction. In the fold test, as applied here, the evolution

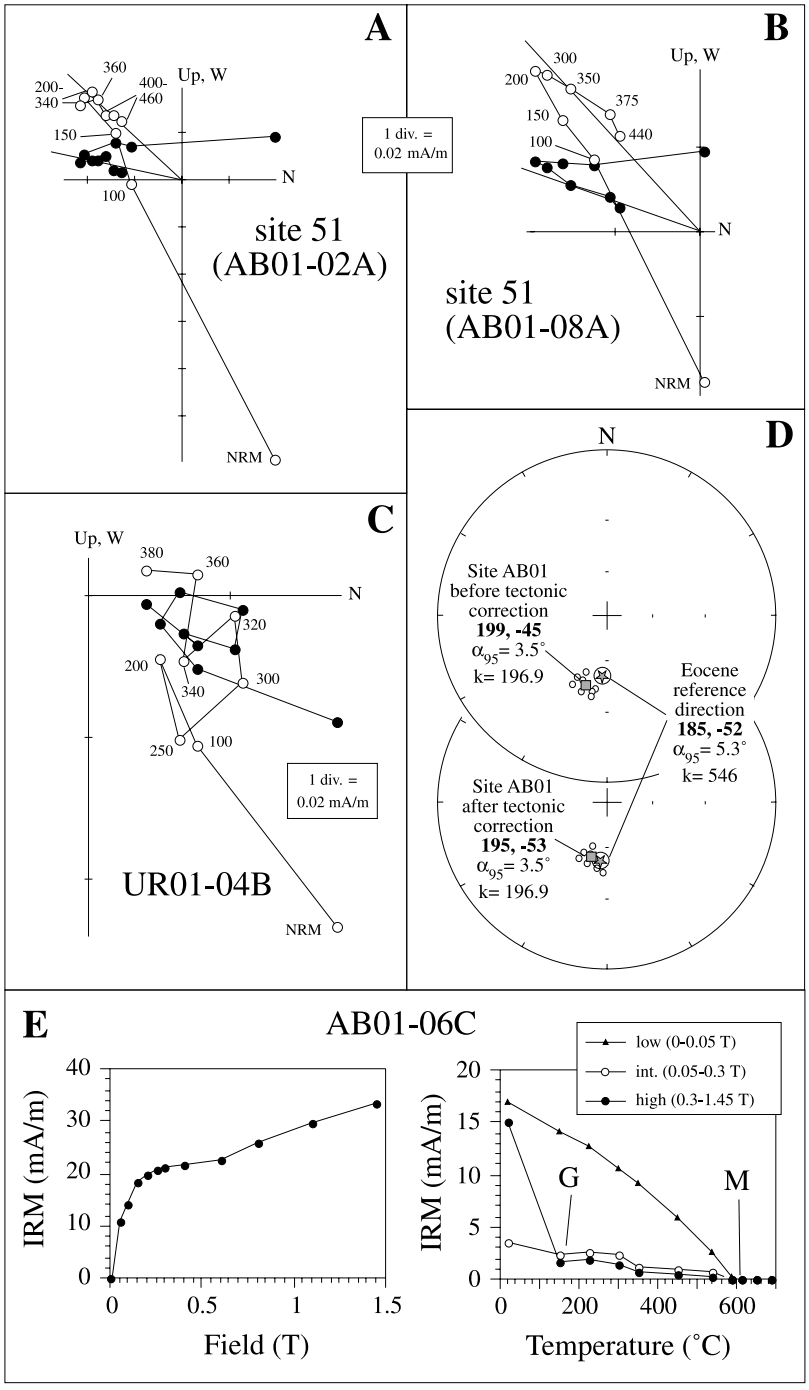

Figure 8. Paleomagnetic results from Eocene limestones. (a and b) Stable NRM demagnetization diagrams representative of site AB01 (site 51 in Figure 2) (all plots for in situ coordinates). (c) Representative example of unstable demagnetization plots for Eocene limestones of the Andia Fault Zone. (d) Equal area projection of ChRM directions from site AB01, before and after tectonic correction. The site mean direction is more similar to the (reversed polarity) Eocene reference direction after restoring the bedding to the horizontal position. All symbols are as in Figure 4. (e) IRM acquisition and thermal demagnetization results of a three-component IRM of representative Eocene limestone samples. G and M indicate the decay of remanence associated with goethite and magnetite, respectively.

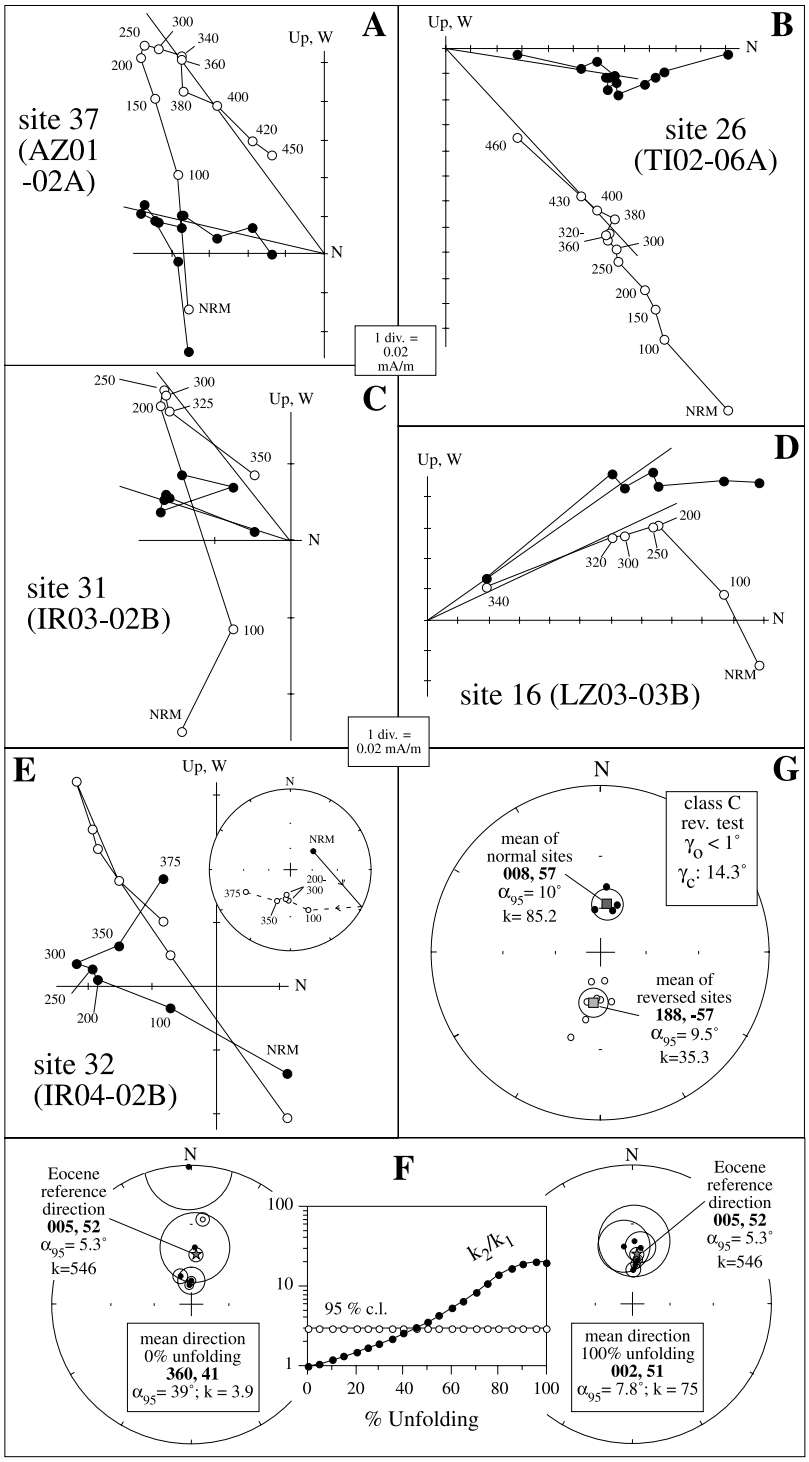

Figure 9. Paleomagnetic results from Eocene marls. (a, b, c, and d) Representative NRM demagnetization diagrams of samples with reliable linear trends directed toward the origin of the plots (all plots for in situ coordinates). (e) NRM demagnetization diagram of a representative sample having unstable behavior above 300°C and a clear, well-developed demagnetization circle. (f) Representative example of fold test (Liédena anticline). Mean directions before and after tectonic correction, together with their associated statistical parameters, are compared with the Eocene reference direction. G is a positive reversal test (Pamplona synclinorium) performed with the site mean ChRM directions of the Eocene marls. Here γ_0 is the angular difference between the normal and reversed mean directions, whereas γ_c represents the critical value of the angle at which the test is considered negative. All symbols are as in Figure 4.

Table 1. Site Mean ChRM Directions and Statistical Parameters[a]

					In Situ		Statistics		Tectonically Corrected		Statistics	
Structural Unit	Age	Site	n/N	LF/DC	Dec	Inc	α_{95}	k	Dec	Inc	α_{95}	k
					Jaca-Pamplona Basin							
Liédena (1)	Eocene	1	6/8	6/0	359	1	17.9	15	352	44	17.9	15
Liédena (1)	Eocene	2	5/8	5/0	9	47	23.6	11.5	2	41	23.6	11.5
Liédena (1)	Eocene	3	8/8	8/0	15	72	10.6	28.3	8	45	10.6	28.3
Liédena (1)	Eocene	4	8/10	8/0	5	−26	3.9	203.4	4	59	3.9	203.4
Liédena (1)	Eocene	5	10/10	10/0	358	72	4.5	114.2	13	60	4.5	114.2
Lumbier (2)	Eocene	6	9/9	9/0	5	68	1.9	722.3	9	42	1.9	722.3
Lumbier (2)	Eocene	7	8/8	8/0	355	81	4.5	151.3	0	49	4.5	151.3
Lumbier (2)	Eocene	8	9/9	9/0	16	37	6.7	59.3	359	40	6.7	59.3
Lumbier (2)	Eocene	9	8/8	8/0	16	36	3.3	289.7	359	47	3.3	289.7
Lumbier (2)	Eocene	10	9/10	9/0	10	24	8.2	40.9	7	52	8.2	40.9
Izaga (3)	Eocene	11	9/11	9/0	356	−43	4.7	121.5	357	60	4.7	121.5
Izaga (3)	Eocene	12	8/8	8/0	13	−29	5.6	98.3	11	62	5.6	98.3
Izaga (3)	Eocene	13	8/10	8/0	34	17	3.6	237.8	37	46	3.6	237.8
Izaga (3)	Eocene	14	7/7	7/0	47	−21	5.8	109.4	52	64	5.8	109.4
Izaga (3)	Eocene	15	7/7	7/0	59	72	4.6	170.8	16	9	4.6	170.8
Izaga (3)	Eocene	16	10/10	10/0	356	−23	10.3	22.8	352	44	10.3	22.8
Izaga (3)	Eocene	17	10/10	10/0	28	19	3.8	163.8	10	48	3.8	163.8
Izaga (3)	Eocene	18	9/10	9/0	15	25	6.5	63.6	4	50	6.5	63.6
Izaga (3)	Eocene	19	9/9	9/0	12	24	19.4	8	9	55	19.4	8
Izaga (3)	Eocene	20	8/9	8/0	14	−24	3.3	276.4	357	76	3.3	276.4
Izaga (3)	Eocene	21	7/11	7/0	4	7	17.7	12.6	358	31	17.7	12.6
Alaiz (4)	Eocene	22	7/7	7/0	282	83	16.6	14.2	344	56	16.6	14.2
Alaiz (4)	Eocene	23	6/10	6/0	25	67	14.4	22.7	14	48	14.4	22.7
Alaiz (4)	Eocene	24	10/10	10/0	305	84	8.7	32.1	355	45	8.7	32.1
Alaiz (4)	Eocene	25	9/9	9/0	5	70	8.3	39.2	0	55	8.3	39.2
Alaiz (4)	Eocene	26	7/7	7/0	5	48	6.5	86.5	8	42	6.5	86.5
Alaiz (4)	Eocene	27	8/9	8/0	13	77	8.7	41.9	20	48	8.7	41.9
Alaiz (4)	Eocene	28	10/10	10/0	110	84	9.8	25.1	17	48	9.8	25.1
Pamplona (5)	Eocene	29	9/12	9/0	359	42	9	33.9	5	47	9	33.9
Pamplona (5)	Eocene	30	10/10	0/10	189	−65	10.5	27	188	−70	10.5	27
Pamplona (5)	Eocene	31	5/10	5/0	189	−51	12.5	38.4	173	−71	12.5	38.4
Pamplona (5)	Eocene	32	6/8	5/5	202	−44	6.5	59.3	200	−34	6.5	59.3
Pamplona (5)	Eocene	33	8/11	8/0	16	4	9.3	36.6	19	57	9.3	36.6
Pamplona (5)	Eocene	34	11/11	0/11	167	−67	9.9	26.2	181	−59	9.9	26.2
Pamplona (5)	Eocene	35	4/11	4/4	185	−10	7.3	63.2	168	−57	7.3	63.2
Pamplona (5)	Eocene	36	7/11	7/0	23	37	13.6	20.6	15	61	13.6	20.6
Pamplona (5)	Eocene	37	10/10	10/0	196	−51	4.5	113.8	196	−56	4.5	113.8
Pamplona (5)	Eocene	38	7/14	0/7	184	−49	13.3	31.1	187	−58	13.3	31.1
Pamplona (5)	Eocene	39	12/15	12/0	23	61	10.6	17.7	353	61	10.6	17.7
Pamplona (5)	Eocene	40	9/13	9/0	206	−32	10.4	25.5	193	−41	10.4	25.5
Añezkar (6)	Eocene	41	9/11	0/9	188	−52	14.5	26.3	218	−53	14.5	26.3
Ibero (7)	Eocene	42	10/13	0/10	181	−56	9.6	32.6	188	−48	9.6	32.6
Ibero (7)	Eocene	43	6/13	6/0	6	−39	7.1	91.2	343	48	7.1	91.2
Ibero (7)	Eocene	44	6/11	6/0	336	45	17.5	15.7	349	40	17.5	15.7
					Andia Fault Zone							
San Donato (8)	Eocene	45	12/14	0/12	177	−52	7.1	45	189	−32	7.1	45
San Donato (8)												
Goñi (9)	Eocene	46	10/14	10/0	17	57	8.3	35.2	15	45	8.3	35.2
Goñi (9)	Santonian	47	11/11	11/0	3	−18	7.1	42	0	43	7.1	42
Goñi (9)	Santonian	48	8/8	8/0	6	0	6.5	73.8	6	57	6.5	73.8
Goñi (9)	Santonian	49	8/10	8/0	11	−19	5.3	111.2	8	47	5.3	111.2
Goñi (9)	Santonian	50	7/9	7/0	3	−12	6.6	84.8	0	37	6.6	84.8
Abarzuza (10)	Eocene	51	10/10	10/0	199	−45	3.5	196.9	195	−53	3.5	196.9
					Miranda-Urbasa Syncline							
Urbasa (11)	Eocene	52	6/12	6/0	17	50	9	56.8	15	51	9	56.8
Urbasa (11)	Maastrichtian	53	6/8	6/0	185	−29	4.4	231.1	193	−42	4.4	231.1
Urbasa (11)	Maastrichtian	54	5/8	5/0	359	43	14.1	30.3	7	63	14.1	30.3
Urbasa (11)	Maastrichtian	55	9/10	9/0	188	−33	4.1	155.5	202	−54	4.1	155.5
Urbasa (11)	Maastrichtian	56	8/10	8/0	186	−34	5.8	99	189	−58	5.8	99

[a]Here n/N is the number of samples used in statistics/demagnetized; LF/DC is the number of linear fit/demagnetization circles used to calculate site mean directions; Dec and Inc are the declination and inclination of the site mean directions; a_{95} and k are the statistical parameters associated with the means. Structural units are numbered according to Figure 2. Statistical parameters are identical in situ and after tectonic correction because bedding is constant at the scale of each paleomagnetic site.

Table 2. Rotation and Flattening for Different Structural Units Compared With Unit Mean Paleomagnetic Directions and the Expected Reference Directions[a]

Structural Unit	Age	s/S	Mean Direction				Reference Direction				
			Dec	Inc	α_{95}	k	Dec	Inc	α_{95}	$R \pm \Delta r$	$F \pm \Delta f$
Jaca-Pamplona Basin											
Liédena (1)	Eocene	5/6	2	51	7.8	75	5	52	5.3	-3 ± 12	0 ± 7
Lumbier (2)	Eocene	5/5	3	46	5.9	170.7	5	52	5.3	-2 ± 9	-6 ± 6
Izaga (3)	Eocene	10/11	10	55	10	24.3	5	52	5.3	$+5 \pm 15$	$+3 \pm 9$
Alaiz (4)	Eocene	7/7	6	49	7.3	69.4	5	52	5.3	$+1 \pm 11$	-3 ± 7
Pamplona (5)	Eocene	12/12	8	57	6.4	47.1	5	52	5.3	$+3 \pm 11$	$+5 \pm 6$
Añezkar (6)	Eocene	1/2	38	53	14.5	26.3	5	52	5.3	$+33 \pm 18$[b]	$+1 \pm 11$
Ibero (7)	Eocene	3/3	355	53	25.8	23.9	5	52	5.3	-10 ± 35	$+1 \pm 20$
Andia Fault Zone											
San Donato (8)	Eocene	1/3	9	32	7.1	45	5	52	5.3	$+4 \pm 9$	-20 ± 6[b]
Goñi (9)	Eocene	1/4	15	45	8.3	35.2	5	52	5.3	$+10 \pm 11$	-7 ± 7
Goñi (9)	Upper Cretaceous	4/5	3	46	10.1	84	1	45	5.8	$+2 \pm 13$	$+1 \pm 9$
Abarzuza (10)	Eocene	1/1	15	53	3.5	196.9	5	52	5.3	$+10 \pm 8$[b]	$+1 \pm 5$
Miranda-Urbasa											
Urbasa (11)	Eocene	1/2	15	51	9	56.8	5	52	5.3	$+10 \pm 12$	-1 ± 7
Urbasa (11)	Upper Cretaceous	4/5	13	54	11.1	69.8	1	45	5.8	$+12 \pm 16$	$+9 \pm 10$

[a]Here s/S is the number of sites used in the statistics/sites analyzed; R ± Dr is the rotation recorded by the ChRM and its associated error calculated after *Demarest* [1983] (positive and negative values indicate clockwise and counterclockwise rotations, respectively); $F \pm \Delta f$ indicates the flattening of the mean inclinations and their associated errors calculated after *Demarest* [1983] (positive and negative values indicate higher and lower values when compared with the reference direction, respectively).
[b]Statistically significant differences.

of the precision parameter (k) is estimated during progressive unfolding (k2) with respect to the initial value (k1) [*McElhinny*, 1964]. The ratio of k2/k1 is then compared with the critical value at the 95% confidence level to assess the statistical significance of the results. The reversal test of *McFadden and McElhinny* [1990] was performed when possible.

4.1. Upper Santonian

[16] The sampled upper Santonian marls and limestones have NRM intensities below 0.1 mA/m. Two stable components of magnetization can be distinguished in the thermal demagnetization results from the upper Santonian marls (Figure 6). A low temperature component unblocks below 300°C. This component has a present-day field direction and thus has little geological relevance. Above 300°C, a ChRM was successfully isolated for four of the studied sites. The ChRM has northerly and shallow negative directions in geographic coordinates and northerly declinations and downward inclinations after structural correction. The absence of reversals and the similar bedding attitude of the sampled sites do not allow for application of field tests. However, we interpret that the ChRM in these rocks is a primary magnetization and does not represent a secondary overprint because (1) the normal polarity ChRM is consistent with a magnetization acquired during the Cretaceous Normal Polarity Superchron in the upper Santonian; (2) site mean directions for in situ coordinates are different from any other later magnetization (e.g., Cretaceous, Tertiary or recent); and (3) site mean inclinations are indistinguishable from the expected reference inclination after bedding correction, but not before such correction (Figure 6d) (Table 2). Rock magnetic measurements indicate that magnetite is the main magnetic carrier of the ChRM in the upper Santonian marls (Figure 6e).

4.2. Upper Maastrichtian

[17] Upper Maastrichtian limestones (5 sites) and marls (1 site) were sampled, of which four sites, all of them limestones, provided reliable results (Figure 7). NRM values are between 0.3 and 5 mA/m. The limestones are characterized by a low temperature component that unblocks below 200°C and carries variable portions of the NRM intensity. This component is consistent with a present-day field overprint. Above 200°C, a ChRM is clearly defined up to 600°C (Figure 7a). Rock magnetic data indicate that goethite and magnetite are the magnetic carriers of the low temperature component and the ChRM, respectively (Figure 7e). In some samples, the low temperature component is weak or even absent, leading to weaker intensities (0.3 to 1 mA/m) and nearly univectorial demagnetization diagrams (Figure 7b). The ChRM in these rocks has reversed polarity, but three samples from the highest part of the sampled section have normal polarity (Figure 7c). Together with reversed polarity directions lower in the stratigraphic sequence, these normal polarity directions provide a consistent match with the geomagnetic polarity time scale in light of biostratigraphic data (top of chron 31r and base of 31n). The origin of the ChRM cannot be assessed by means of fold tests because all sites have similar bedding attitudes. However, the presence of samples with opposite polarities seems to exclude the possibility of a

secondary origin. The test performed yields positive results (Figure 7d) and suggests that the ChRM in the Maastrichtian limestones is a primary magnetization.

4.3. Eocene Limestones

[18] One out of the 7 sampled sites from Eocene limestones has stable paleomagnetic behavior (Figure 8). The NRM at this site (0.2 mA/m) consists of two stable components. A low temperature magnetization is unblocked below 200°C and carries the main fraction of the NRM. This component is parallel to the present-day field in the area. Above 300°C, a ChRM is identified (Figures 8a and 8b). Rock magnetic data indicate that goethite and magnetite are the magnetic carriers of the low temperature component and the ChRM, respectively (Figure 8e). The ChRM of the Eocene limestones was successfully isolated at only one site, so no field tests constrain the age of the remanence. At this site, the ChRM has reversed polarity for in situ coordinates. After tilt correction, the inclination steepens so that it is closer to the expected Eocene inclination (Figure 8d) (Table 2). Other Tertiary limestone formations in the Pyrenees have been shown to record dual polarity magnetizations that allowed retrieval of magnetostratigraphic data [*Pascual et al.*, 1992; *Pujalte et al.*, 1995]. These observations suggest that the ChRM in the Eocene limestones is a primary direction.

4.4. Eocene Marls

[19] Thermal demagnetization of more than 500 samples (55 sites) from Eocene marls indicates weak NRM intensities (between 0.1 to 0.6 mA/m). Two stable remanence components are identified after removal of a magnetization probably acquired during drilling or sample storage (Figure 9). A low temperature component typically unblocks below 300°C. It has normal polarity before structural correction and is interpreted as a present-day field overprint. A ChRM is defined above 250–300°C. This component is not completely unblocked at 450°–460°C (Figures 9a and 9b), although in some cases the maximum unblocking temperature is below 350°C (Figures 9c and 9d). This observation and several rock-magnetic experiments indicate that both magnetite and magnetic iron sulphides (most likely pyrrhotite) contribute to the ChRM [*Larrasoaña et al.*, 2003a]. The ChRM has been successfully isolated in about 65% of the analyzed samples and has both normal and reversed polarities after structural correction. Reliable site mean directions have been calculated for 47 out of the 55 studied sites. The incremental fold test has been performed using ChRM directions from 6 structural units that include 43 sites. The best grouping of ChRM directions occurs between 80% and 95% of unfolding. However, the grouping is not significantly different than at 100% unfolding, which indicates that the ChRM was essentially acquired prior to folding (Figure 9f). The reversal test performed on the ChRM site mean directions from the Pamplona syncline is positive at the 95% confidence level (Figure 9g). Different magnetostratigraphic studies focused on the Eocene marls of the eastern sector of the Jaca-Pamplona basin have shown that the polarity reversal pattern in the marls is consistent with available biostratigraphic data [*Hogan and Burbank*, 1996; *Pueyo et al.*, 2002]. These observations indicate that the ChRM in the Eocene marls represents a primary magnetization.

5. Discussion

[20] The mean paleomagnetic direction for each structural unit has been calculated by averaging the directions from the different sites according to age. Mean directions have been compared with the expected reference direction for the area in order to determine the magnitude of vertical axis rotations (R). The Eocene reference direction (D = 5°, I = 52°, α_{95} = 5.3°; k = 546) has been recalculated from the Eocene Iberian paleopole of *Taberner et al.* [1999]. The reference direction for the upper Cretaceous (D = 1°, I = 45°, α_{95} = 5.8°; k = 172.3) has been recalculated after averaging the upper Cretaceous paleopoles available for stable Iberia [see *Van der Voo*, 1993 and references therein]. Confidence limits for the rotations (Δr) have been calculated following *Demarest* [1983]. Flattening of the inclination (F) and its confidence limit (Δf) [*Demarest*, 1983] have been also calculated for every structural unit (Table 2). It is noticeable that, with the exception of the San Donato syncline, all of the mean inclinations are statistically indistinguishable from the reference inclination. The pattern of vertical axis rotations for the different structural units is depicted in Figure 10a. The error limits on the paleomagnetic directions usually span the reference direction and therefore indicate the absence of significant vertical axis rotations. The only two structural units where significant rotations have been found correspond to a fault-bounded unit (Abarzuza block) within the AFZ and a small, steeply (26°) plunging fold (Añezkar syncline) to the north of the Iza diapir. The Añezkar syncline records a large rotation of +33 ± 18° (+ denotes clockwise), whereas the Abarzuza has shows a small rotation of +10 ± 8°. The results for both localities are based on one site only and might lack of statistical significance. However, no-significant tectonic rotations are reported for 9 out of 11 structural units studied, which include 53 out of 56 sites where reliable paleomagnetic results were obtained. These units are widespread throughout the studied area. We therefore conclude that vertical axis rotations on either side and across the PF did not occur during the Tertiary. Tectonic rotations in thrust belts are mainly driven by gradients in tectonic shortening [*Allerton*, 1998]. The lack of rotations in the studied area is compatible with the similar values of tectonic displacement estimated along the Pamplona and Urbasa transects.

[21] A variety of different models for block rotations associated with strike-slip faults have been proposed by different authors. It is useful to consider simplified kinematic models (Figure 10b) in order to gain insight into the complexities that strike-slip faults can develop [*Twiss and Moores*, 1992]. Two models [*McKenzie and Jackson*, 1983; *Ron et al.*, 1984] predict the existence of generalized tectonic rotations of the same sense as the slip in the shear zone. The model proposed by *Garfunkel* [1989] also predicts generalized rotations, although they are in the opposite

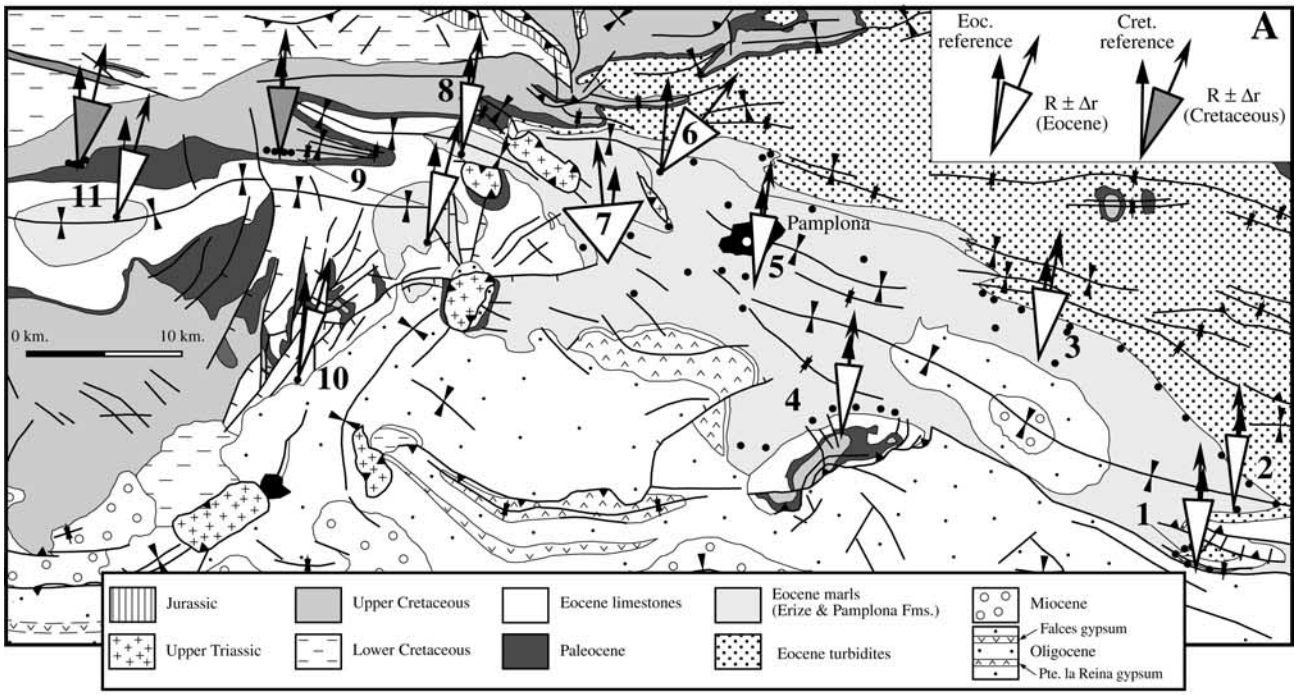
A
Eoc. reference
Cret. reference
R ± Δr (Eocene)
R ± Δr (Cretaceous)
Pamplona
0 km.
10 km.
1
2
3
4
5
6
7
8
9
10
11
Jurassic
Upper Triassic
Upper Cretaceous
Lower Cretaceous
Eocene limestones
Paleocene
Eocene marls (Erize & Pamplona Fms.)
Eocene turbidites
Miocene
Falces gypsum
Oligocene
Pte. la Reina gypsum

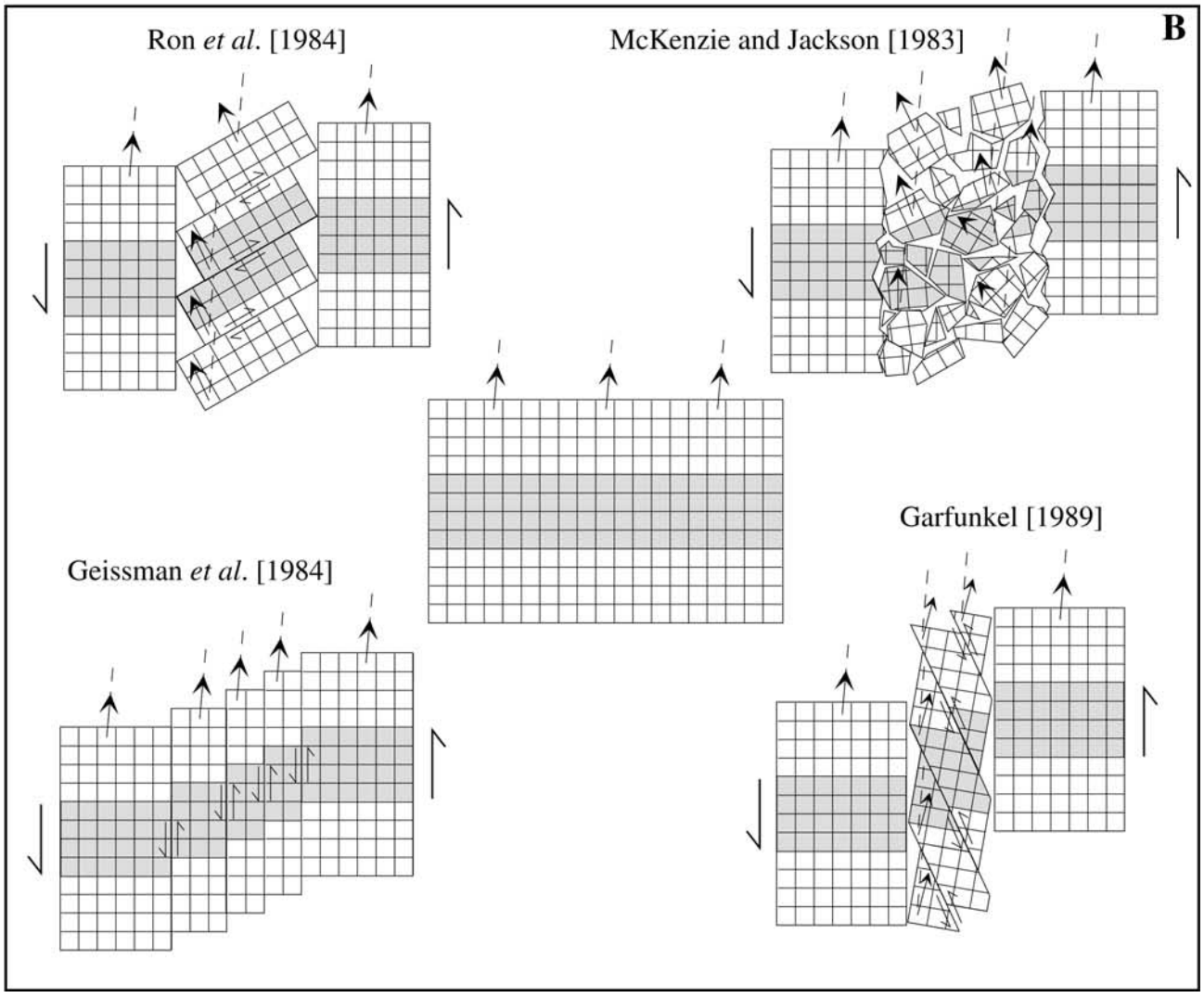
B
Ron *et al*. [1984]
McKenzie and Jackson [1983]
Garfunkel [1989]
Geissman *et al*. [1984]

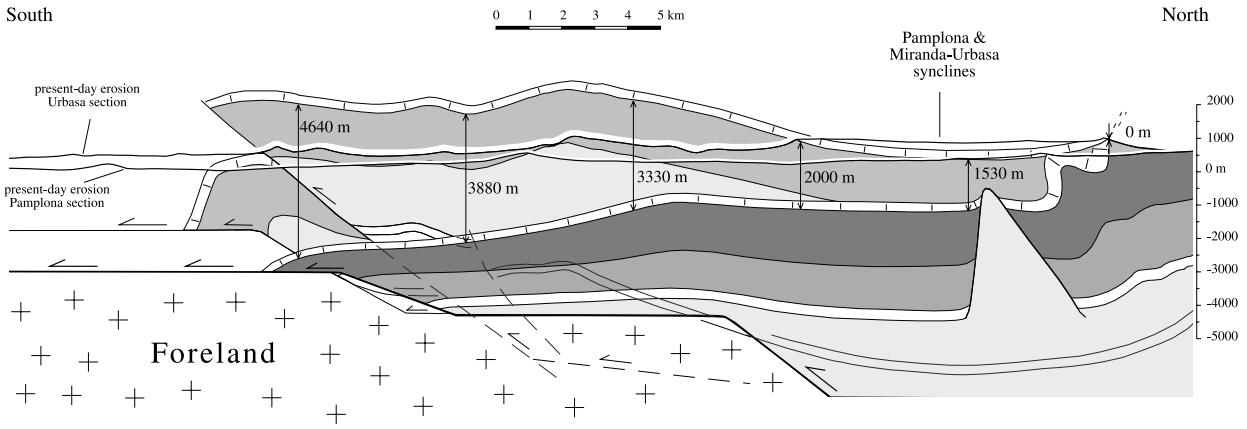

Figure 11. Schematic image of the present-day attitude of Mesozoic sequences along the Pamplona (shaded patterns as in Figure 4) and Urbasa transects (shaded colors), plotted along a common vertical scale.

sense with respect to the main strike-slip movement. None of these models can be applied to the PF because our data indicate an absence of tectonic rotations associated with the PF. The only model that satisfies our paleomagnetic results is that proposed by *Geissman et al.* [1984], in which tectonic displacement is accommodated by a set of parallel faults involving no rotation. However, the model does not account for the geometry and kinematics of the AFZ, because faults in this system show no strike-slip, but mainly dip-slip, displacements.

[22] One explanation for the lack of tectonic rotations in the study area is that the Mesozoic-Tertiary cover is detached from the basement at the upper Triassic plastic levels, and therefore that the strike-slip movement of the basement fault might not be transferred to the cover. However, this possibility does not explain why most of the arguments claiming for a strike-slip movement of the PF are based on structural features observed in the cover rocks (e.g., the Triassic salt diapirs and the AFZ). The overall geological features of the area are still to be explained.

[23] It is useful to recall the arguments that led to the interpretation of the PF as a strike-slip fault. Concerning a possible sinistral offset between the North Pyrenean and Leiza Faults, it has to be demonstrated that these two faults formed a single structure at the onset of the Tertiary deformation before they can be used as a reliable marker of strike-slip movements. Geophysical, stratigraphic, structural and paleomagnetic evidence [*Peybernès and Souquet*, 1984; *Puigdefàbregas and Souquet*, 1986; *García-Mondéjar*, 1996; *Casas et al.*, 1997; *Larrasoaña et al.*, 2003b] indicate that the Iberian-European Mesozoic plate boundary can be envisaged as an intricate set of pull-apart basins and basement blocks bounded by several families of strike-slip faults, which comprise a wide domain of deformation on top of a thinned crust. Therefore there is no need for continuity between the North Pyrenean and Leiza Faults because they can be regarded individually as some of the several faults accommodating deformation at the plate boundary [*Larrasoaña et al.*, 2003b]. In fact, the North Pyrenean Fault cannot be traced west of Arette (0°25′W) [*Hall and Johnson*, 1986] and the arguments supporting its westward continuation are unclear. The N-S offset of the Moho reported by *Gallart et al.* [1981] west of Arette reflects variations in the thickness of the crust in the Iberian and European plates after the Pyrenean orogen [*ECORS-Pyrenees Team*, 1988], but it does not necessarily have a causal relationship with the position, or even the absence, of a Mesozoic structure such as the NPF at the surface. On the other hand, structural reconstructions indicate that listric, normal faults, rather than a vertical structure such as the NPF, were active west of Arette during the Mesozoic [*Teixell*, 1996]. In addition, *Souriau and Pauchet* [1998] suggested that the alignment of earthquakes west of Arette could be related to the low-angle thrust that host the Alduides massif, rather than to a vertical structure such as the NPF. Further evidence claiming against the continuation between the North Pyrenean and Leiza Faults come from Cretaceous reconstructions of Iberia prior to opening of the Bay of Biscay [*García-Mondéjar*, 1996].

[24] On the other hand, offset of the south Pyrenean basal thrust [*Froutè*, 1988] cannot be considered as evidence for

Figure 10. (opposite) (a) Geological sketch map of the studied area showing the mean declination of the ChRM for every structural unit. The cones represent the confidence angle of the rotations. (b) Kinematic models of block rotations associated with a left-lateral strike-slip fault.

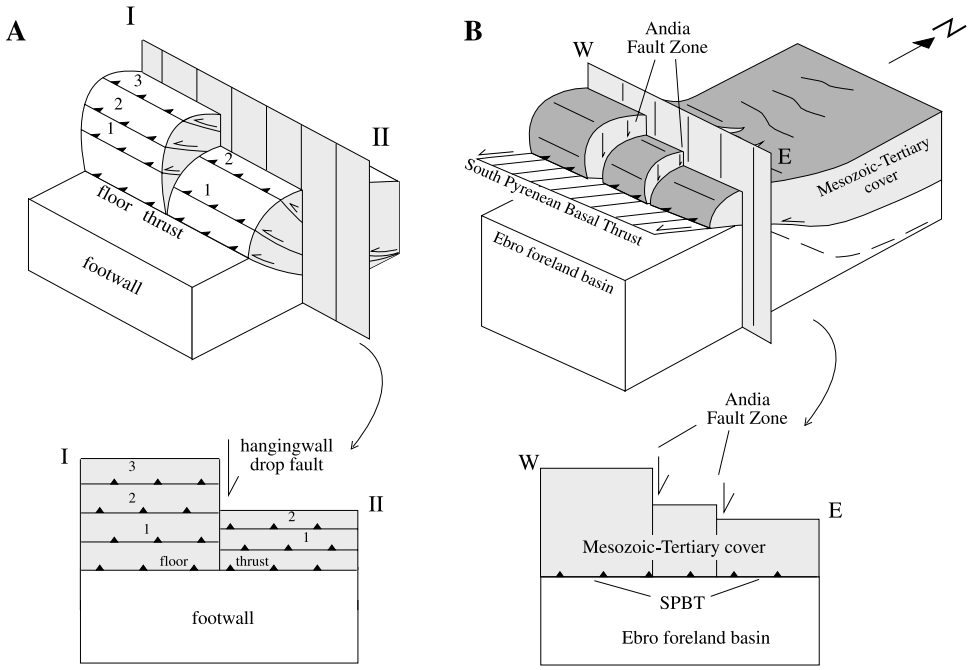

Figure 12. (a) Model of a "hanging wall drop fault" according to *Elliott and Johnson* [1980] and (b) proposed model for the Pamplona Fault, in which the formation of hanging wall drop faults (Andia Fault Zone) is conditioned by differences in cover thickness on both sides of the Pamplona Fault.

sinistral displacement along the PF because the SPBT does not emerge to the surface. Other evidence for dextral movement along the PF is also questionable. The curvature of the Ulzama, Aralar and Arberoue structures (Figure 1b) may not represent any kinematic feature. At the western termination of the Labourd massif, curvature in the opposite sense to that of the Arberoue structure is found. However, no major structure such as the PF, with the opposite sense of motion, has been identified there. Moreover, the trace of the Roncesvalles thrust and some other Tertiary structures near the Ulzama and Aralar structures are not curved across the PF, raising further doubts about the validity of these geometric features. An interpretation for dextral offset of the Paleozoic basement [*Turner*, 1996] is faced with the difficulty of determining the pre-Tertiary arrangement of basement units at both sides of the PF, especially considering the complex Cretaceous paleogeography at the ancient plate boundary. On the other hand, curvature of Eocene facies belts across the PF [*Payros*, 1997] can be explained in terms of variable progradation and retrogradation of the sedimentary sequences on both sides of the PF (in order to keep pace with differential tectonic loading in the internal parts of the orogen), rather than to a real horizontal displacement across the fault.

[25] Perhaps the strongest argument for rejecting hypotheses of strike-slip movement of the PF during the Pyrenean orogeny is the fact that Paleocene and Eocene marine sediments located along the axis of the Jaca-Pamplona basin form a continuous outcrop that can be traced toward the west, in the Miranda-Urbasa syncline, across the trace of the fault (see Figures 1 and 2). In view of the above evidence, we suggest that a new model is necessary to explain the kinematics of the PF.

6. A New Model for the Pamplona Fault

[26] The two key aspects for unraveling the Tertiary kinematics of the PF are (1) to consider the control exerted by the geometry of the Mesozoic extensional faults in the thickness of the Cretaceous sedimentary sequences and (2) the influence of such geometries and thicknesses in the resulting configuration of the hanging wall of the SPBT after the cover was inverted and transported toward the south. Coupling between tectonics and stratigraphy is illustrated in Figure 11, where the two cross sections are plotted against a common vertical scale. The vertical offset observed at the base of the Tertiary sediments on both sides of the PF results mainly from the differential uplift of the cover when it was transported toward the south, although the different position of the basal detachment on both sides of the PF may also account for part of this offset.

[27] It has been proposed that, during piggy-back thrusting, local duplex development may result in laterally variable thicknesses between the roof and the floor thrusts [*Elliott and Johnson*, 1980] (Figure 12a). This would cause the formation of "hanging wall drop faults" parallel to the tectonic transport direction. Such faults differ from lateral ramps in that they only have a dip-slip displacement, as they do not accommodate differential thrust displacement but only differential uplift caused by variable duplex thickness [*Elliott and Johnson*, 1980]. The "hanging wall drop fault" model can be applied to our study area with the only

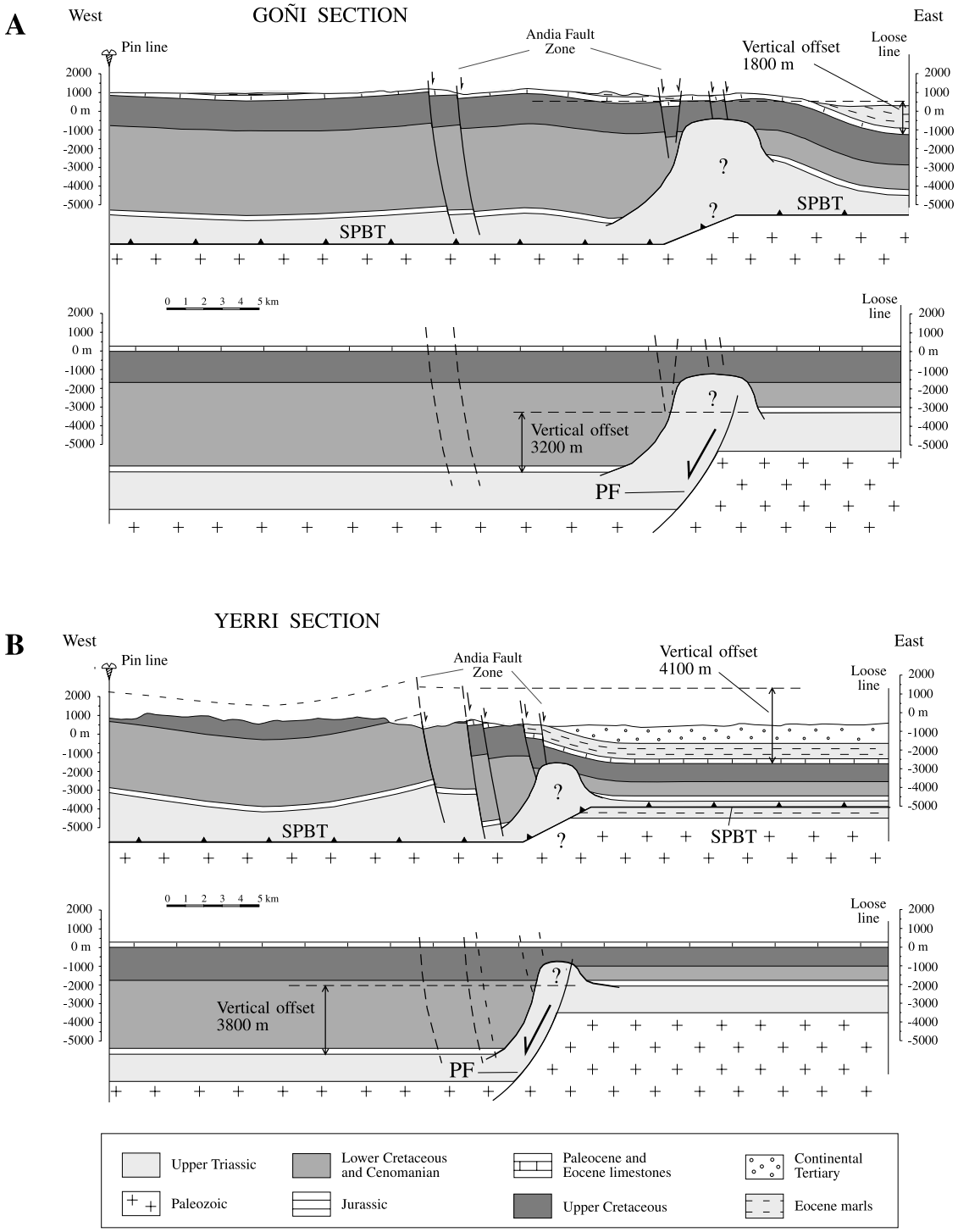

Figure 13. Restoration of the cross sections depicted in Figure 5 at the beginning of the Paleocene (prior to development of Tertiary thrusting). The vertical offset across the PF during the Cretaceous extension and differential uplift experienced by the cover during the Tertiary inversion are shown in the restored and original cross sections, respectively.

difference that variations in uplift on both sides of the PF are mainly caused by changes in the stratigraphic thickness rather than by different degrees of local duplex stacking (Figures 12b and 13). This model satisfactorily explains the overall structural, stratigraphic and paleomagnetic data obtained in the studied area. The Mesozoic-Tertiary cover was transported about ~15 km toward the south along the SPBT. Lack of differential shortening associated with this

displacement did not produce any vertical axis rotations (as indicated by paleomagnetic data) or strike-slip displacements along the PF (as indicated by structural observations). As the cover was transported over the footwall, the PF behaved as a passive structure that was inactively transported on the hanging wall of the SPBT and separated units with similar tectonic displacements but with different stratigraphic sequences. Variations in stratal thickness on both sides of the PF resulted in differential uplift and led to local extension, which was accommodated by the hanging wall drop faults of the AFZ. These normal faults have maximum vertical displacements toward the south (Figure 13b), where the vertical offset occurred across the PF during the Cretaceous extension is compensated by differential uplift of the cover during the Tertiary inversion. The vertical displacement accommodated by the AFZ diminishes progressively to the north (Figure 13a), as differential Tertiary uplift on both sides of the PF decreases in the same direction and only compensates a small fraction of the Cretaceous extension. Eventually, the faults of the AFZ disappear in the area where the cover rocks were not transported over the footwall ramp and differential uplift did not occur (Figure 2).

[28] Well-known field examples of transverse zones that accommodate tectonic inversion along segments of a thrust and fold belt with different prethrusting sedimentary thickness include the Segre Fault in the central eastern Pyrenees [*Vergès*, 1993], the Tiburon Ridge in the Barbados accretionary complex, and the Caussols-Grasse Transverse Zone in the French Alps [see *Calassou et al.*, 1993]. However, the PF differs from these cases in that variable prethrusting sedimentary thicknesses are not accommodated by anastomosed oblique ramps formed within the transverse zone, as it occurs in the central eastern Pyrenees and the French Alps [*Calassou et al.*, 1993; *Vergès*, 1993] and has been reported in analogue modeling studies [*Calassou et al.*, 1993]. Instead, such differences are accommodated by the formation of (extensional) hanging wall drop faults parallel to the transport direction. We speculate that the differences between the PF and other field examples are related to the importance of differential prethrusting sedimentary thickness on both sides of the transverse fault and its orientation with respect to the shortening direction.

7. Conclusions

[29] Paleomagnetic results obtained from Cretaceous and Tertiary sedimentary rocks on both sides of the PF indicate that no vertical axis rotations occurred around the fault during the Tertiary. Together with structural and stratigraphic data, these results indicate that the PF did not behave as a strike-slip fault, but as a transverse fault that separated segments of the Pyrenean orogen with different tectonostratigraphic evolution. During the Mesozoic, the PF behaved as a transfer fault that separated two segments of the Pyrenean rift where differences in the amount and/or style of extension occurred. Tertiary compression took place parallel to previous extension, leading to inversion of the Mesozoic basins. The presence of a detachment level and the striking variations in the Mesozoic sequences on both sides of the PF controlled the kinematics of the fault, that behaved as a hanging-wall drop fault according to the model shown in Figures 12 and 13. The lack of vertical axis rotations and variations of shortening accommodated on both sides of the fault, together with the lack of strike-slip displacements and the absence of associated deep-seated seismicity, suggests that previous interpretations claiming a prominent role of the PF in terms of Pyrenean deep-crustal structure have been overstated.

[30] Although formation of hanging wall drop faults in connection with differential prethrusting thickness have been previously suggested by *Boyer and Elliott* [1982], the Pamplona Fault is, to our knowledge, the first detailed case of such a type of transverse structure reported in the literature. Considering the importance of inherited structural features in the formation and development of transverse faults [e.g., *Milani and Davison*, 1988; *Calassou et al.*, 1993; *Clemson et al.*, 1997; *Moustafa*, 1997; *Acocella et al.*, 1999], we suspect that closer examination of transverse structures in other mountain belts where tectonic inversion occurred might lead to the recognition of situations that can be explained using our model. Before doing so, however, an integrated paleomagnetic, structural and stratigraphic approach is necessary to assess the role and kinematics of transverse faults during basin inversion processes.

[31] **Acknowledgments.** We are indebted to our colleagues of the Paleomagnetic Laboratory of the Ludwig-Maximilians Universität (Munich), where a substantial part of the paleomagnetic analysis was carried out, for their hospitality, technical assistance and discussion at the early stages of this study. J. Dinarès-Turell kindly provided paleomagnetic results from two of the studied sites and also contributed to the improvement of this work with his comments and criticisms. L. M. Martínez-Torres, A. M. Casas-Sainz, A. Pocoví, A. P. Roberts, and A. Sussman are also gratefully thanked for invaluable discussions and help at different stages during this study. Charles Aubourg and an anonymous reviewer are also acknowledged for their comments and criticism on an earlier version of the manuscript. This work was supported by two predoctoral grants of the Navarra Government and MEC to J. C. L. and E. L. P., the DGES (Projects PB96-0815 and PB97-0997) and a DFG-CSIC joint project.

References

Acocella, V., C. Faccena, R. Funiciello, and F. Rossetti, Sand-box modelling of basement-controlled transfer zones in extensional domains, *Terra Nova*, *11*, 149–156, 1999.

Allerton, S., Geometry and kinematics of vertical-axis rotations in fold and thrust belts, *Tectonophysics*, *299*, 15–30, 1998.

Alvarez-Marrón, J., E. Rubio, and M. Torné, Subduction-related structures in the north Iberian margin, *J. Geophys. Res.*, *102*, 22,497–22,511, 1997.

Bailey, R. C., and H. C. Halls, Estimate of confidence in paleomagnetism direction derived from mixed remagnetization circle and direct observational data, *J. Geophys.*, *54*, 174–182, 1984.

Boillot, G., and J. Malod, The north and north-west Spanish continental margin: A review, *Rev. Soc. Geol. Esp.*, *1*, 295–316, 1988.

Boyer, S. E., and D. Elliott, Thrust systems, *AAPG Bull*, *66*, 1196–1230, 1982.

Brinkmann, R., and H. Logters, Die Diapire der spanischen Westpyrenaen in ihres Vorlandes, *Geol. Jahrb. Beih.*, *66*, 1–20, 1967.

Brun, J. P., and M. O. Beslier, Mantle exhumation at passive margins, *Earth Planet. Sci. Lett.*, *142*, 161–173, 1996.

Buchanan, J. G., and P. G. Buchanan (Eds.), *Basin Inversion*, *Geol. Soc. Spec. Publ.*, *88*, 596 pp., 1995.

Butler, R. W. H., The terminology of structures in thrust belts, *J. Struct. Geol.*, *4*, 239–246, 1982.

Canudo, J. I., E. Molina, J. Riveline, J. Serra-Kiel, and M. Sucunza, Les événements biostratigraphyques de la zone prépyrénée d'Aragón (Espagne), de l'Eocene moyen á l'Oligocéne inférieur, *Rev. Micropaleontol.*, *31*, 15–29, 1988.

Calassou, S., C. Larroque, and J. Malavieille, Transfer zones of deformation in thrust wedges: An experimental study, *Tectonophysics*, *221*, 325–344, 1993.

Casas, A., P. Kearey, L. Rivero, and C. R. Adam, Gravity anomaly map of the Pyrenean region and a comparison of the deep geological structure of the western and eastern Pyrenees, *Earth Planet. Sci. Lett.*, *150*, 65–78, 1997.

Casas-Sainz, A. M., I. Gil, B. Leránoz, H. Millán, and J. L. Simón, Quaternary reactivation of flexural-slip folds by diapiric activity: Example from the western Ebro Basin (Spain), *Geol. Rundsch.*, *83*, 853–867, 1994.

Choukroune, P., Tectonic evolution of the Pyrenees, *Annu. Rev. Earth Planet. Sci.*, *20*, 143–158, 1992.

Clemson, J., J. Cartwright, and J. Booth, Structural segmentation and the influence of basement structure on the Namibian passive margin, *J. Geol. Soc. London*, *154*, 477–482, 1997.

Cooper, M. A., and G. D. Williams (Eds.), *Inversion Tectonics*, *Geol. Soc. Spec. Publ.*, *44*, 376 pp., 1989.

Cortés-Gracia, A. L., and A. M. Casas-Sainz, Fosas neógenas asociadas a la reactivación de pliegues en el borde sur de la Sierra de Cantabria (Alava-Navarra), *Geogaceta*, *21*, 81–84, 1997.

Debroas, E., La flysch noir Albo-Cénomanien témoin de la structuration Albienne à Sénonienne de la zone nord-Pyrénéene en Bigorre (Hautes Pyrénées France), *Bull. Soc. Geol. Fr.*, *8*, 273–285, 1990.

Demarest, H. H., Error analysis for the determination of tectonic rotation from paleomagnetic data, *J. Geophys. Res.*, *88*, 4321–4328, 1983.

Ebinger, C. J., B. R. Rosendahl, and D. J. Reynolds, Tectonic model of the Malawi Rift, Africa, *Tectonophysics*, *141*, 215–235, 1987.

ECORS-Pyrenees Team, The ECORS deep seismic survey across the Pyrenees, *Nature*, *331*, 508–511, 1988.

Elliott, R., and J. A. Johnson, Structural evolution in the northern part of the Moine thrust belt of NW Scotland, *Trans. R. Soc. Edinburgh Earth Sci.*, *71*, 69–96, 1980.

Engeser, T., and W. Schwentke, Towards a new concept of the tectogenesis of the Pyrenees, *Tectonophysics*, *129*, 233–242, 1986.

Faci, E., J. Castiella, J. del Valle, A. García, A. Díaz, J. M. Salvany, P. Cabra, J. Ramírez del Pozo, and A. Meléndez, Mapa geológico de Navarra, scale 1:20,0000, 142 pp., Gobierno de Navarra, Navarra, Spain, 1997.

Fisher, R. A., Dispersion on a sphere, *Proc. R. Soc. London, Ser. A*, *217*, 295–305, 1953.

Froutè, J. Y., Le rôle de l'accident d'Estella dans l'histoire géologique Crétacé supérieur à Miocéne des bassins Navarro-Alavais (Espagne du Nord), Ph.D. thesis, 231 pp., Univ. de Pau, Pau, France, 1988.

Gallart, J., E. Banda, and M. Daigniéres, Crustal structure of the Paleozoic axial zone of the Pyrenees and transition to the North Pyrenean Zone, *Ann. Geophys.*, *37*, 457–480, 1981.

García-Mondéjar, J., Plate reconstruction of the Bay of Biscay, *Geology*, *24*, 635–638, 1996.

Garfunkel, Z., Regional deformation by block translation and rotation, in *Paleomagnetic Rotations and Continental Deformation*, *Nato ASI Ser., Ser. C.*, vol. 254, edited by C. Kissel and C. Laj, pp. 181–208, Kluwer Acad., Norwell, Mass., 1989.

Geissman, J. W., J. T. Callian, J. S. Oldow, and S. E. Humphries, Paleomagnetic assessment of oroflexural deformation in west-central Nevada and significance for emplacement of allochtonous assemblages, *Tectonics*, *3*, 179–200, 1984.

Hall, C. A., and J. A. Johnson, Apparent western termination of the North Pyrenean Fault and tectonostratigraphic units of the western north Pyrenees, France and Spain, *Tectonics*, *5*, 607–627, 1986.

Harding, T. P., R. C. Vierbuchen, and N. Christie-Blick, Structural styles, plate-tectonic settings and hydrocarbon traps of divergent (transtensional) wrench faults, in *Strike-Slip Deformation, Basin Formation and Sedimentation*, edited by K. T. Biddle and N. Christie-Blick, *Spec. Publ. Soc. Econ. Paleont. Mineral.*, *37*, 51–77, 1985.

Hogan, P. J., and D. W. Burbank, Evolution of the Jaca piggyback basin and emergence of the external Sierra, southern Pyrenees, in *Tertiary Basins of Spain*, edited by P. F. Friend and C. J. Dabrio, pp. 153–160, Cambridge Univ. Press, New York, 1996.

Instituto Geológico y Minero de España (IGME), Logroño, *Mapa Geol. Esp. Escala 1:50,000, 204*, 1977a.

Instituto Geológico y Minero de España (IGME), Lodosa, *Mapa Geol. Esp. Escala 1:50,000, 205*, 1977b.

Instituto Geológico y Minero de España (IGME), Gulina, *Mapa Geol. Esp. Escala 1:50,000, 115*, 1978a.

Instituto Geológico y Minero de España (IGME), Eulate, *Mapa Geol. Esp. Escala 1:50,000, 139*, 1978b.

Instituto Geológico y Minero de España (IGME), Pamplona, *Mapa Geol. Esp. Escala 1:50,000, 141*, 1978c.

Instituto Geológico y Minero de España (IGME), Salvatierra, *Mapa Geol. Esp. Escala 1:50,000, 113*, 1987a.

Instituto Geológico y Minero de España (IGME), Alsasua, *Mapa Geol. Esp. Escala 1:50,000, 114*, 1987b.

Instituto Geológico y Minero de España (IGME), Estella, *Mapa Geol. Esp. Escala 1:50,000, 140*, 1987c.

Instituto Geológico y Minero de España (IGME), Viana, *Mapa Geol. Esp. Escala 1:50,000, 171*, 1987d.

Instituto Geológico y Minero de España (IGME), Allo, *Mapa Geol. Esp. Escala 1:50,000, 172*, 1987e.

Instituto Geológico y Minero de España (IGME), Tafalla, *Mapa Geol. Esp. Escala 1:50,000, 173*, 1987f.

Instituto Geológico y Minero de España (IGME), Peralta, *Mapa Geol. Esp. Escala 1:50,000, 206*, 1987g.

Instituto Geológico y Minero de España (IGME), Documentos sobre la geología del subsuelo de España, vol. IV, Ebro-Pirineos, Madrid, 1990.

Kirschvink, J. L., The least-squares line and plane and the analysis of palaeomagnetic data, *Geophys. J. R. Astron. Soc.*, *62*, 699–718, 1980.

Larrasoaña, J. C., J. M. Parés, J. del Valle, and H. Millán, Triassic paleomagnetism from the western Pyrenees revisited: Implications for the Iberian-Eurasian Mesozoic plate boundary, *Tectonophysics*, *362*, 161–182, 2003a.

Larrasoaña, J. C., J. M. Parés, and E. L. Pueyo, Stable Eocene magnetization carried by magnetite and magnetic iron sulphides in marine marls (Pamplona-Arguis Formation, southern Pyrenees, N Spain), *Stud. Geophys. Geod.*, *47*, 237–254, 2003b.

Laubscher, H. P., Large-scale, thin-skinned thrusting in the southern Alps: Kinematic models, *Geol. Soc. Am. Bull.*, *96*, 710–718, 1985.

Liesa, C., Fracturación y campos de esfuerzos compresivos alpinos en la Cordillera Ibérica y el NE peninsular, Ph.D. thesis, 611 pp., Univ. of Zaragoza, Zaragoza, Spain, 2000.

Lister, G. S., M. A. Etheridge, and P. A. Symonds, Detachment faulting and the evolution of passive continental margins, *Geology*, *14*, 246–250, 1986.

Martínez-Torres, L. M., El Manto de los Mármoles (Pirineo Occidental): Geología estructural y evolución geodinámica, Ph.D. thesis, 294 pp., Univ. of Pais Vasco, San Sebastián, Spain, 1989.

Martínez-Torres, L. M., Corte balanceado de la Sierra de Cantabria (Cabalgamiento de la Cuenca Vasco-Cantabrica sobre la Cuenca del Ebro), *Geogaceta*, *14*, 113–115, 1993.

Mattauer, M., Les traits structuraux essentiels de la chaine Pyrénéenne, *Rev. Geogr. Phys. Geol. Dyn.*, *2*, 3–12, 1968.

McClay, K. R. (Ed.), *Thrust Tectonics*, 433 pp., Chapman and Hall, New York, 1992.

McClay, K. R., and S. Khalil, Extensional hard linkages, eastern Gulf of Suez, Egypt, *Geology*, *26*, 563–566, 1998.

McDougall, J. W., and S. H. Kahn, Strike-slip faulting in a foreland fold and thrust belt: The Kalabagh fault and western fault range, Pakistan, *Tectonics*, *9*, 1061–1075, 1990.

McElhinny, M. W., Statistical significance of the fold test in paleomagnetism, *Geophys. J. R. Astron. Soc.*, *8*, 338–340, 1964.

McFadden, P. L., and M. W. McElhinny, The combined analysis of remagnetization circles and direct observations in palaeomagnetism, *Earth Planet. Sci. Lett.*, *87*, 161–172, 1988.

McFadden, P. L., and M. W. McElhinny, Classification of the reversal test in palaeomagnetism, *Geophys. J. Int.*, *103*, 725–729, 1990.

McKenzie, D. P., and J. A. Jackson, The relationship between strain rates, crustal thickening, paleomagnetism, finite strain, and fault movement within a deforming zone, *Earth. Planet. Sci. Lett.*, *65*, 184–202, 1983.

Milani, E. J., and I. Davison, Basement control and transfer tectonics in the Reconcavo-Tucano-Jatoba rift, northeast Brazil, *Tectonophysics*, *154*, 41–70, 1988.

Millán, H., E. Pueyo, M. Aurell, A. Luzón, B. Oliva, B. Martínez-Peña, and J. Pocoví, Actividad tectónica registrada en los depósitos terciarios del frente meridional del Pirineo central, *Rev. Soc. Geol. Esp.*, *13*, 279–300, 2000.

Mitra, S., Three-dimensional geometry and kinematic evolution of the Pine Mountain thrust system, southern Appalachians, *Geol. Soc. Am. Bull.*, *100*, 72–95, 1988.

Moustafa, A. R., Controls on the development and evolution of transfer zones: The influence of basement structure and sedimentary thickness in the Suez rift and Red Sea, *J. Struct. Geol.*, *19*, 755–768, 1997.

Müller, J., and P. Roger, L'evolution des Pyrénées (domaine central et occidental). Le segment Hercynien, la chaine de fond alpine, *Geol. Alp.*, *53*, 141–191, 1977.

Muñoz, J. A., Evolution of a continental collision belt: ECORS-Pyrenees crustal balanced cross-section, in *Thrust Tectonics*, edited by K. R. McKlay, pp. 235–246, Chapman and Hall, New York, 1992.

Muñoz, J. A., C. Puigdefàbregas, and J. M. Fontboté, Orógenos alpinos, El Pirineo; Introducción, in *Geología de España-Libro Jubilar J. M. Ríos*, vol. 2, pp. 161–167, Inst. Geol. y Minero de Esp., Madrid, 1983.

Muñoz-Jiménez, A., and A. M. Casas-Sainz, The Rioja trough (N Spain): Tectosedimentary evolution of a symmetric foreland basin, *Basin Res.*, *9*, 65–85, 1997.

Pascual, J. O., J. M. Parés, C. Langereis, and J. D. A. Zijderveld, Magnetostratigraphy and rock magnetism of the Ilerdian stratotype at Tremp, Spain, *Phys. Earth Planet. Inter.*, *74*, 139–157, 1992.

Payros, A., El Eoceno de la cuenca de Pamplona: Estratigrafía, facies y evolución paleogeográfica, Ph.D. thesis, 403 pp., Univ. of País Vasco, San Sebastián, Spain, 1997.

Peybernès, B., and P. Souquet, Basement blocks and tectosedimentary evolution in the Pyrenees during Mesozoic times, *Geol. Mag.*, *121*, 397–405, 1984.

Pueyo, E. L., H. Millán, and A. Pocoví, Rotation velocity of a thrust: A paleomagnetic study in the external Sierras (southern Pyrenees), *Sediment. Geol.*, *146*, 191–208, 2002.

Puigdefàbregas, C., and P. Souquet, Tecto-sedimentary cycles and depositional sequences of the Mesozoic and Tertiary from the Pyrenees, *Tectonophysics*, *129*, 173–205, 1986.

Puigdefàbregas, C., J. A. Muñoz, and J. Vergès, Thrusting and foreland basin evolution in the southern

Pyrenees, in *Thrust Tectonics*, edited by K. R. McClay, pp. 247–254, Chapman and Hall, New York, 1992.

Pujalte, V., J. I. Baceta, J. Dinarès-Turell, X. Orue-Etxebarria, J. M. Parés, and A. Payros, Biostratigraphic and magnetostratigraphic intercalibration of latest Cretaceous and Paleocene depositional sequences from the deep-water Basque basin, western Pyrenees, Spain, *Earth Planet. Sci. Lett.*, *136*, 17–30, 1995.

Pulgar, J., J. Gallart, G. Fernández-Viejo, A. Pérez-Estaún, J. Alvarez-Marrón, and ESCIN Group, Seismic image of the Cantabrian mountains in the western extension of the Pyrenees from integrated ESCIN reflection and refraction data, *Tectonophysics*, *246*, 1–19, 1996.

Rat, P., The Basque-Cantabrian basin between the Iberian and European plates: Some facts but still many problems, *Rev. Soc. Geol. Esp.*, *1*, 327–348, 1988.

Riba, O., and M. J. Jurado, Reflexiones sobre la geología de la parte occidental de la Depresión del Ebro, *Acta Geol. Hisp.*, *27*, 177–193, 1992.

Riba, O., S. Reguant, and J. Villena, Ensayo de síntesis estratigráfica y evolutiva de la cuenca del Ebro, in *Geología de España-Libro Jubilar J. M. Ríos*, vol. 2, pp. 131–159, Inst. Geol. y Minero de Esp., Madrid, 1983.

Ron, H., R. Freund, and Z. Garfunkel, Block rotation by strike-slip faulting: Structural and paleomagnetic evidence, *J. Geophys. Res.*, *89*, 6256–6270, 1984.

Schoeffler, J., Les transverales Basco-Landaises, *Bull. Cent. Rech. Explor. Prod. Elf Aquitaine*, *6*, 257–263, 1982.

Serrano, A., and W. Martínez del Olmo, Tectónica salina en el dominio Cántabro-Navarro: Evolución, edad y origen de las estructuras salinas, in *Libro Homenaje a Rafael Soler*, pp. 39–53, Asoc. de Geól. y Geofís. Esp. del Petróleo, Madrid, 1989.

Soler, R., J. López-Vilchez, and Z. Riaza, Petroleum geology of the Bay of Biscay, in *Petroleum Geology of the Continental Shelf of North-West Europe*, edited by L. V. Illing and G. D. Hobson, pp. 474–482, Inst. of Pet., London, 1981.

Souriau, A., and H. Pauchet, A new synthesis of Pyrenean seismicity and its tectonic implications, *Tectonophysics*, *290*, 221–244, 1998.

Srivastava, S. P., W. R. Roest, L. C. Krovacs, K. Schouten, K. Klitgord, J. Verhoef, and R. Macnab, Iberian plate kinematics: A jumping plate boundary between Eurasia and Africa, *Nature*, *344*, 756–759, 1990.

Taberner, C., J. Dinarès-Turell, J. Giménez, and C. Docherty, Basin in-fill architecture and evolution from magnetostratigraphic cross-basin correlations in the southeastern Pyrenean foreland basin, *Geol. Soc. Am. Bull.*, *111*, 1144–1174, 1999.

Teixell, A., The Ansó transect of the southern Pyrenees: Basement and cover thrust geometries, *J. Geol. Soc. London*, *153*, 301–310, 1996.

Thomas, W. A., Controls on location of transverse zones in thrust belts, *Eclogae Geol. Helv.*, *83*, 727–744, 1990.

Turner, J. P., Switches in subduction direction and the lateral termination of mountain belts: Pyrenees-Cantabrian transition, Spain, *J. Geol. Soc. London*, *153*, 563–571, 1996.

Twiss, R. J., and E. M. Moores, *Structural Geology*, 532 pp., W. H. Freeman, New York, 1992.

Van der Voo, R., *Paleomagnetism of the Atlantic, Tethys and Iapetus Oceans*, 411 pp., Cambridge Univ. Press, New York, 1993.

Vergès, J., Estudi geològic del vessant Sud del Pirineu Oriental i Central: Evolució en 3D, Ph.D. thesis, 203 pp., Univ. of Barcelona, Barcelona, Spain, 1993.

Vergès, J., and J. Garcia-Senz, Mesozoic evolution and Cenozoic inversion of the Pyrenean rift, in *Peritethyan Rift Wrench Basins and Passive Margins*, edited by P. A. Ziegler et al., *Mem. Mus. Natl. Hist. Nat.*, *186*, 187–212, 2001.

Wernicke, B., Uniform-sense normal simple shear of the continental lithosphere, *Can. J. Earth Sci.*, *22*, 108–125, 1985.

Wiedmann, A., Itineraire géologique a travers le Crétacé moyen des chaines Vascogotiques et Celtiberiques (Espagne du nord), *Cuad. Geol. Iber.*, *5*, 127–214, 1979.

J. del Valle, Santo Domingo 3, 48280 Lekeitio, Spain.

J. C. Larrasoaña, Southampton Oceanography Centre, European Way, Southampton SO14 3ZH, UK. (jcl1@soc.soton.ac.uk)

H. Millán, Department of Earth Sciences, University of Zaragoza, Pedro Cerbuna 12, Zaragoza 50009, Spain.

J. M. Parés, Department of Geological Sciences, University of Michigan, 2534 C. C. Little Building, Ann Arbor, MI 48109, USA.

E. L. Pueyo, Laboratoire de Méchanismes de Transfert en Géologie, Université Paul Sabatier, 31062 Toulouse Cedex 4, France.